Pyridine-functionalized carbazole donor and benzophenone acceptor design for thermally activated delayed fluorescence emitters in blue organic light emitting diodes

P. Rajamalli, Diego Rota Martir, Eli Zysman-Colman*
Organic Semiconductor Centre, EaStCHEM School of Chemistry, University of St Andrews, St Andrews, Fife, KY16 9ST, UK, Fax: +44-1334 463808; Tel: +44-1334 463826

Abstract. In this paper we report a new molecular design approach for blue emitting thermally activated delayed fluorescence (TADF) molecules. The two novel TADF emitters, (4-(3,6-di(pyridin-3-yl)-9H-carbazol-9-yl)phenyl)(phenyl)methanone (**3PyCzBP**), and (4-(3,6-diphenyl-9H-carbazol-9-yl)phenyl)(phenyl)methanone (**4PyCzBP**) possess a pyridine-functionalized carbazole donor and a benzophenone acceptor. Both compounds shows broad charge-transfer emission in DCM with a λ_{max} at 497 nm and a photoluminescence quantum yield, Φ_{PL} of 56% for **3PyCzBP** and a λ_{max} at 477 nm and a Φ_{PL} of 52% for **4PyCzBP**. The Φ_{PL} decreased to 18% and 10%, respectively for **3PyCzBP** and **4PyCzBP** in the presence of O_2 confirming that triplet states involved in emission. The PMMA doped (10 wt%) films show blue-shifted emission with λ_{max} at 450 and 449 nm for **3PyCzBP** and **4PyCzBP**, respectively. The maximum Φ_{PL} of 23.4% is achieved for these compounds in PMMA doped film. Difference in energy between the singlet and triplet excited states (ΔE_{ST}) is very small at 0.06 eV and 0.07 eV for **3PyCzBP** and **4PyCzBP**, respectively. Multilayer organic light emitting diode devices fabricated using these molecules as emitters show that the maximum efficiency (EQE_{max}) of the blue devices is 5.0%.

Keywords: TADF, OLEDs, benzophenone, blue emitter, delayed fluorescence.

***Third Author, E-mail: eli.zysman-colman@st-andrews.ac.uk

Introduction

Organic light-emitting diodes (OLEDs) are acquiring significant and increasing attention as a technology in flat panel displays, smart watches, smart phones and large-screen televisions.(1, 2) The maximum internal quantum efficiency (IQE) is typically 25% for OLEDs using conventional fluorescent dopants.(3) The IQE can be increased from 25% to 100% by harvesting triplet excitons using phosphorescent emitters.(4-6) However, phosphorescent emitters almost always are organometallic complexes based on noble metals such as Ir or Pt. These metals are some of the rarest naturally occurring elements on Earth and the environmental sustainability and toxicity remain detracting features of these materials. Further, although many blue

phosphorescent materials have been developed, the OLEDs employing these materials as emissive dopants have short device operational lifetimes and show red-shifted Commission Internationale de l'Éclairage (CIE) coordinates (y coordinate is >0.25), which precludes them from commercial use.(7-9) Thus, the development of highly efficient blue-emitting materials is desired to overcome these problems. Triplet−triplet annihilation TTA material-based devices are limited to maximum 62.5%.(10, 11) Unlike TTA, thermally activated delayed fluorescence, TADF, or E-type fluorescence materials in OLEDs can reach an internal quantum efficiency of 100% by harvesting both singlet and triplet excitons.(12) In 2012, Adachi *et al*(13) demonstrated that OLED external quantum efficiency, EQE, based on organic TADF emitters could reach beyond the theoretical maximum 5%, assuming a light outcoupling efficiency of 20%. Since this seminal report, over 400 distinct TADF emitters have been developed for high performance OLEDs.(14) The TADF mechanism requires a small singlet−triplet energy gap (ΔE_{ST}) in order to thermally up-convert the triplet excitons to the singlet excited state *via* a reverse intersystem crossing (RISC). In terms of a molecular design this is achieved by reduced the overlap integral of the frontier molecular orbitals (i.e. the highest occupied molecular orbital, HOMO, and the lowest unoccupied molecular orbital, LUMO) in the molecule. This HOMO and LUMO separation is frequently achieved by combining the donor and acceptors counterpart in the molecule such that they are electronically decoupled. However, a reduction in ΔE_{ST} is accompanied by a low oscillator strength, *f*, for the charge transfer transition, which inevitably reduces the quantum efficiency of the device. Therefore, there is a tradeoff between the ΔE_{ST} and *f* in order to optimize the photoluminescence quantum yield of the emitter and therefore the efficiency of the device. It now becomes evident that TADF emitter design is a critical factor to achieve high-efficiency TADF OLEDs. Although various red, green, and blue TADF emitters

had been developed,(14-16) the optimum molecular design for blue-emitting TADF compounds is not well understood, and guidelines for the rational molecular design are highly desired. One strategy for HOMO localization, and by extension small ΔE_{ST}, is for wide dispersion of the HOMO through the presence of multiple donor groups or extended donors. Although the EQEs of the OLEDs were found to increase, the color coordinates were red-shift significantly from blue to green, which is a detracting feature of this strategy for the development of blue TADF materials.(17-20) Typically, extended or dendronized donors are constituted of a central carbazole heterocycle decorated on the periphery with addition carbazole or diphenylamine donor units.

Herein, we report a new molecular design for blue TADF emitters where in contrast to the conventional strategies, we modified the carbazole donors with weak electron-withdrawing pyridine rings. Two novel TADF emitters, **4PyCzBP** and **3PyCzBP**, have been designed, synthesized and characterized and OLED devices fabricated. These emitters are composed of a dipyridyl carbazole donor moiety and a benzophenone (BP) unit as the acceptor (Fig. **1**). The presence of these additional pyridine rings on the carbazole donor weaken the electron-donating nature of the core carbazole thereby reinforcing the blue emission of the material both in solution and in thin film. The photophysical properties of these compounds have been studied and the maximum photoluminescence quantum yield 23.4% is achieved for these compounds in PMMA doped film with a λ_{max} around 450 nm. Multilayer OLED devices fabricated using these molecules as dopants in a high energy DPEPO host show maximum EQEs of the blue devices as high as 5.0%.

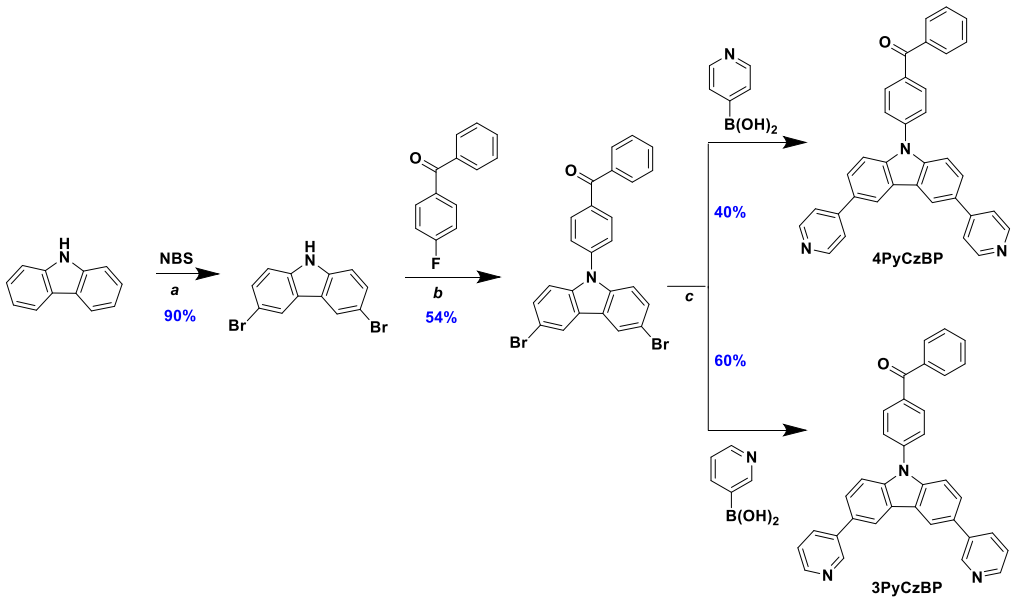

Scheme **1**. Synthesis of **4PyCzBP** and **3PyCzBP**. Reagents and conditions: [a] MeCN, 273 to 298 K, 2 h. [b] DMF, KO^{t}Bu (1 equiv.), 150 °C, 19 h. [c] 1,4-dioxane:H_2O (4:1 v/v), Cs_2CO_3 (6 equiv.), $Pd(PPh_3)_4$ (0.1 equiv.), 110 °C, 48 h. All reactions were conducted under an N_2 atmosphere.

Results and Discussion

The synthetic route for the TADF emitters **3PyCzBP** and **4PyCzBP** and are given in Scheme **1** and were synthesized with overall yields of 19% and 29%, respectively, in three steps. The detailed synthetic procedures and characterization data are reported in the experimental section. Density functional theory (DFT) calculations were performed for these compounds, which show spatial separation of the HOMO and LUMO for both emitters. As illustrated in Fig. **1**, the HOMOs of **3PyCzBP** and **4PyCzBP** are mainly distributed over the dipyridylcarbazolyl donor group and slightly extended to the bridging phenyl ring. The LUMOs are mostly localized on the benzophenone acceptor. The small overlap between HOMO-LUMO observed, which is important for a small ΔE_{ST}. The time-dependent DFT (TDDFT) calculated singlet-triplet energy gaps (ΔE_{ST}) are 0.45 eV and 0.41 eV, respectively, for **4PyCzBP** and **3PyCzBP**. The calculated ΔE_{ST} values suggest that these materials may be TADF in nature.(21) In order to assess the effect

of the presence of the pyridine units on the optoelectronic properties of the emitters we modelled the reference compound **CzBP** and **PyCz**. This compound shows a shallower HOMO level (5.76 eV) than both **3PyCzBP** (5.83 eV) and **4PyCzBP** (5.99 eV). In addition, the pyridine units on the carbazole donor increase the oscillator strength of the S_0-S_1 transition and slightly reduce the ΔE_{ST} values (Fig. **1** and Tables 6-13 (appendix)).

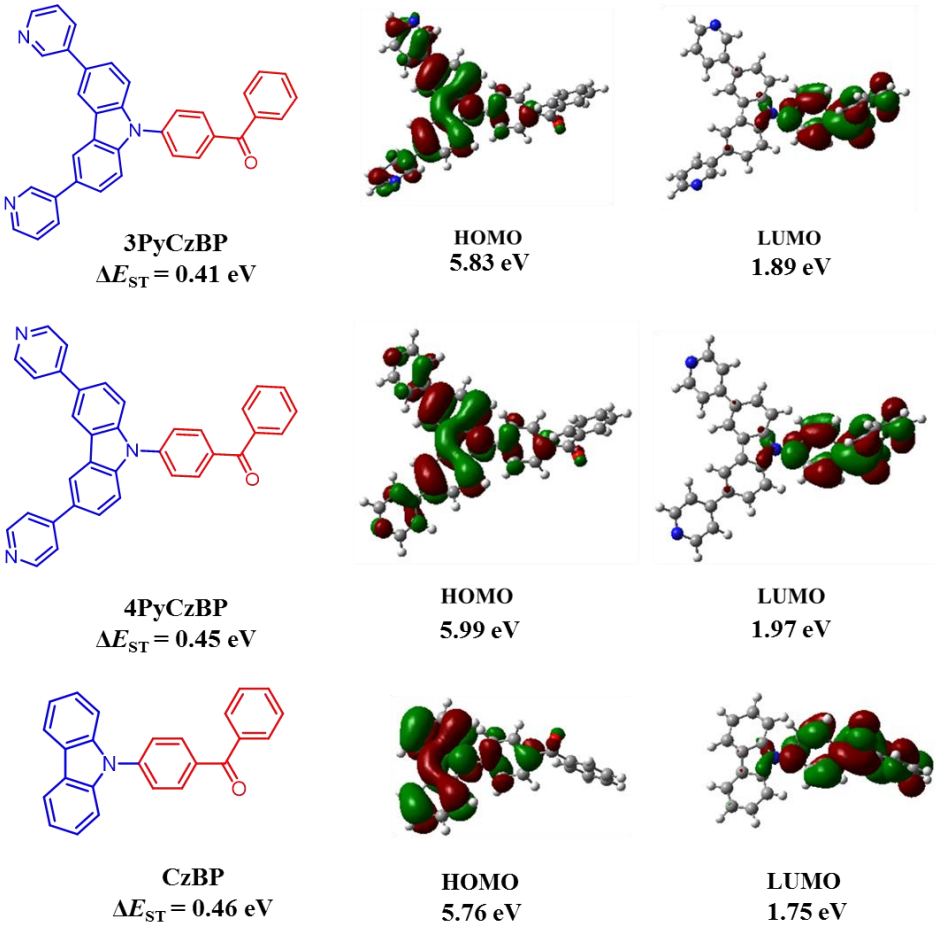

Fig. **1** Structure of TADF emitters and corresponding DFT calculated HOMO and LUMO electron density distribution.

Optoelectronic Characterization

The absorption and emission spectra of **3PyCzBP** and **4PyCzBP** were measured in DCM and are shown in Fig. **2**, and the data are summarized in Tables **1** and **2**. Both compounds exhibit a broad

charge transfer (CT) absorption band at 356 and 326 nm for **3PyCzBP** and **4PyCzBP**, respectively, assigned as an intramolecular charge transfer (ICT) band from the carbazole moiety to the benzophenone based on TDDFT. The absorption bands around 300 nm are localized on the pyridylcarbazole donor, in line with the calculated absorption band found at 293 nm for **PyCz** by TDDFT (Table **8** (appendix)). Electrochemical measurements on **3PyCzBP**, and **4PyCzBP** were carried out in MeCN. The cyclic voltammetry (CV) and differential pulse voltammetry (DPV) traces are shown in Fig. **8** (appendix). The oxidation waves are only pseudo-reversible with oxidation potentials for **3PyCzBP** of (E_{pa} = 1.69 V vs SCE) and for **4PyCzBP** of (E_{pa} = 1.71 V vs SCE). The calculated HOMO levels ($E_{HOMO\ vs\ Fc/Fc+} = E_{pa} + 4.8$ eV) are -6.11 eV and -6.13 eV for **3PyCzBP** and **4PyCzBP**, respectively. These values are deeper than the reported values for ketone-derived carbazole-based D-A-D and D-A systems (-5.7 eV),(18, 21) demonstrating the electron-withdrawing and HOMO-stabilizing nature of the pyridine rings. This analysis is entirely consistent with the DFT calculations (Fig. **1**).

Both compounds show broad emission spectra in DCM with a λ_{max} at 497 nm and a photoluminescence quantum yield, Φ_{PL}, of 56% for **3PyCzBP** and a λ_{max} at 477 nm and a Φ_{PL} of 52% for **4PyCzBP** (Fig. **2**). Notably, the Φ_{PL} decreased to 18% and 10%, respectively for **3PyCzBP** and **4PyCzBP** in the presence of O_2, thereby confirming that triplet states are implicated in the emission, which are readily quenched in the presence of oxygen. A blue-shift of 844 cm^{-1} (20 nm) in the emission spectra of **4PyCzBP** is observed compared to **3PyCzBP** due to the greater electron-withdrawing character of the 4-pyridyl ring that is conjugated into the Cz donor system. The emission is blue-shifted when the compounds are dispersed in PMMA films (10 wt%) with λ_{max} at 450 and 449 nm for **3PyCzBP** and **4PyCzBP**, respectively. The Φ_{PL}

values under N_2 are 23.4% and 21.0%, which decreased in the presence of O_2 to 19.1% and 17.3% for **3PyCzBP** and **4PyCzBP**, respectively, an indication that triplet states are populated upon photoexcitation in the film.(22) The ΔE_{ST} values in 10 wt% doped PMMA films calculated from the peak maxima as well as the onset of the fluorescence and phosphorescence spectra for **3PyCzBP** and **4PyCzBP**. The ΔE_{ST} values based on the emission maxima are 0.06 and 0.07 eV for **3PyCzBP** and **4PyCzBP**, respectively, while the estimate of ΔE_{ST} based on the emission onset is even smaller at 0.03 eV and 0.05 eV, respectively (Fig. **3**). The percent contribution of the delayed fluorescence to the overall emission decay for **3PyCzBP** and **4PyCzBP** are 18.3% and 17.7%, respectively.

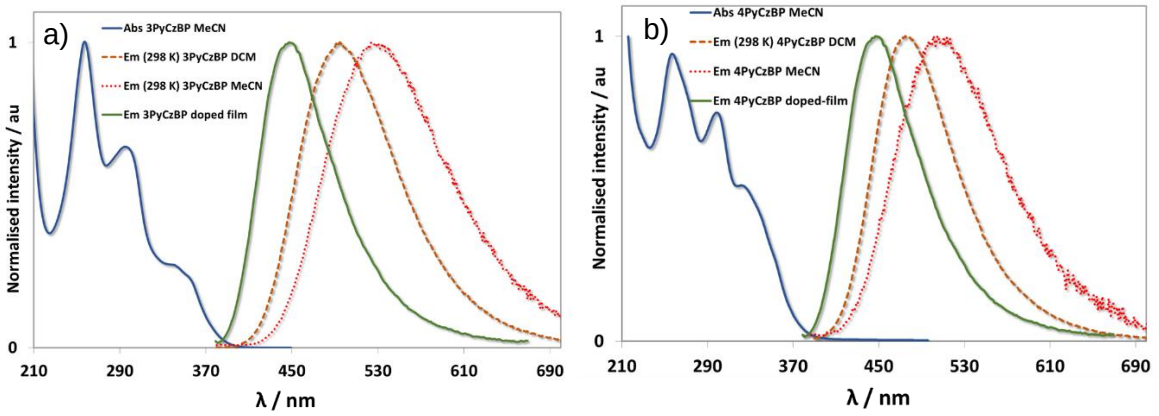

Fig. **2** Photophysical properties of a) **3PyCzBP** and b) **4PyCzBP**, normalised UV-Vis spectrum of collected in MeCN at 298 K (blue line) and normalised emission spectra collected in DCM at 298 K (dashed orange line), in MeCN at 298 K (dotted red line) and as spin-coated PMMA-doped films (green) (10 wt%) on quartz substrate.

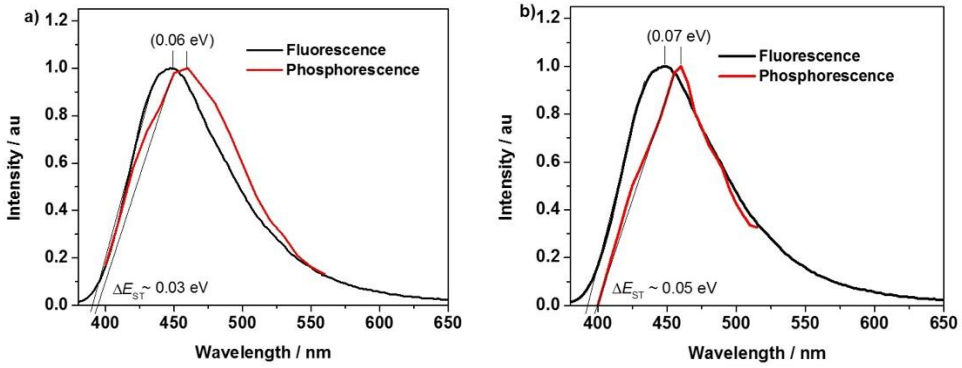

Fig. **3** Normalised fluorescence and phosphorescence emission spectrum of a) **3PyCzBP** and b) **4PyCzBP** on PMMA-doped film formed (10 wt% of compound) by spin-coating deposition on quartz substrate. Fluorescence and phosphorescence spectra measured at 293 and 77 K, respectively and phosphorescence spectra are measured with a 10 μs delay time.

Table **1**. UV-Vis absorption data of **3PyCzBP** and **4PyCzBP**

Compound	λ_{max} [a] / nm [ε / $\times 10^3$ M^{-1} cm^{-1}][b]
3PyCzBP	258 [54.8], 298 [47.3], 342 [24.4], 356 [23.7]
4PyCzBP	258 [50.8], 301 [43.9], 326 [34.2]

[a] UV-Vis absorption in DCM with a concentration on the order of 10^{-5} – 10^{-6} M collected at 298 K. [b] Concentration-independent molar extinction coefficients.

Table **2**. Photophysical properties of **3PyCzBP** and **4PyCzBP**

	λ_{em} (nm)		Φ_{PL} (%)		τ_{PL} [d] (ns)
	DCM[a]	Film[b]	Film[b,c]		Film[b]
			N_2	O_2	Vacuum
3PyCzBP	497	450	23.4	19.1	28 (0.71), 546.5 (0.07), 12,545 (0.22)
4PyCzBP	477	449	21.0	17.3	33.5 (0.75), 611.3 (0.05), 6320 (0.20)

[a] Measurements in degassed DCM at 298 K (λ_{exc} = 360 nm). [b] PMMA doped thin films (10 wt%) formed by spin-coating on a quartz substrate. [c] Values obtained using an integrating sphere under nitrogen or oxygen (λ_{exc} = 360 nm). [d] Values in parentheses are pre-exponential weighting factors, in relative % intensity, of the emission decay kinetics (λ_{exc} = 378 nm, 300 K).

The transient PL decay characteristics of **3PyCzBP** and **4PyCzBP** 10 wt% doped PMMA films under vacuum are shown in Fig. **4** and the data are summarized in Table **2**. Prompt fluorescence, τ_p, of 28.0 ns and 33.5 ns, respectively, for **3PyCzBP** and **4PyCzBP** were determined by TCSPC measurements. The delayed fluorescence lifetimes showed biexponential decay kinetics with τ_d, of 0.55 μs, 12.54 μs for **3PyCzBP** and 0.61 μs, 6.32 μs for **4PyCzBP**, an indication of reverse intersystem crossing (RISC) from the triplet to the singlet excited state. Variable temperature transient PL spectra are shown in Fig. **4** and Fig. **9** (appendix) and the data summarised in Table **5** (appendix). As expected for organic materials emitting *via* a TADF mechanism, τ_d for both compounds gradually increased with increasing temperature due to the thermally activated RISC. These transient PL decays corroborate the TADF assignment of the emission in doped PMMA films.

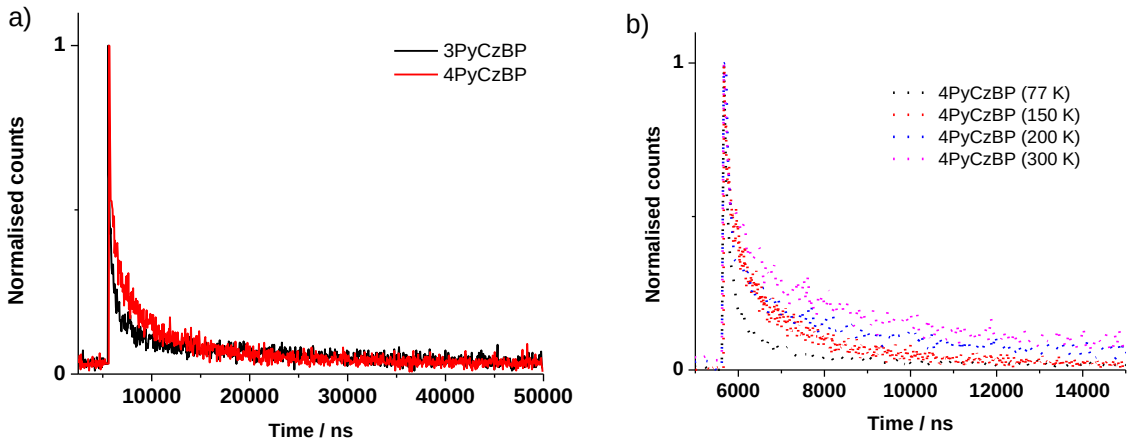

Fig. **4** a) Emission decay of **3PyCzBP** and **4PyCzBP** collected at 300 K (λ_{exc} = 378 nm) in PMMA-doped thin films (10 wt% of emitter), b) Emission decay of **4PyCzBP** (λ_{exc} = 378 nm) collected as PMMA-doped thin film (10 wt% of emitter) at 77 K (in blue), at 150 K (in yellow), at 200 K (in grey) and at 300 K (in orange). Thin films are formed by spin-coating deposition on quartz substrate

Electroluminescence

To evaluate the performance of **3PyCzBP** and **4PyCzBP** in OLEDs, we fabricated multilayer devices using these dopants. The schematic representation of the device architecture and molecular structures of the materials used in the devices are shown in Fig. **5**. Devices A and B, employing, respectively, **3PyCzBP** and **4PyCzBP** as the dopant were fabricated using the following layers: ITO/NPB (30 nm)/TAPC (20 nm)/*m*CP (10)/DPEPO: Dopant (7 wt%) (30 nm)/ TPBi (40 nm)/LiF (0.8 nm)/Al (100 nm), respectively. In these devices, *N*,*N*′-bis(1-naphthyl)-*N*,*N*′-diphenyl-1,1′-biphenyl-4,4′-diamine (NPB) acts as the hole injection material, 1,1-bis[4-[*N*,*N*′-di(ptolyl)amino]phenyl] cyclohexane (TAPC) is the hole transporting material, and 1,3-bis(*N*-carbazolyl)benzene (*m*CP) is the an exciton blocking layer and 3,3-di(9*H*-carbazol-9-yl)biphenyl (*m*CBP) is the host material, while 2,2′,2"-(1,3,5-benzenetriyl)-tris(1-phenyl-1-*H*-benzimidazole) (TPBi) is the electron-transporting material. The electroluminescent properties of these devices are displayed in Fig. **6** and **7**, and the data are summarized in Table **3**. Here, DPEPO is used as a host as it has the most suitable HOMO level (6.1 eV) given the deep HOMO levels of these emitters (~6.1 eV); bipolar host materials, including BCPO have too shallow HOMO levels (~ 5.7 eV) and therefore are not suitable host materials for these emitters.

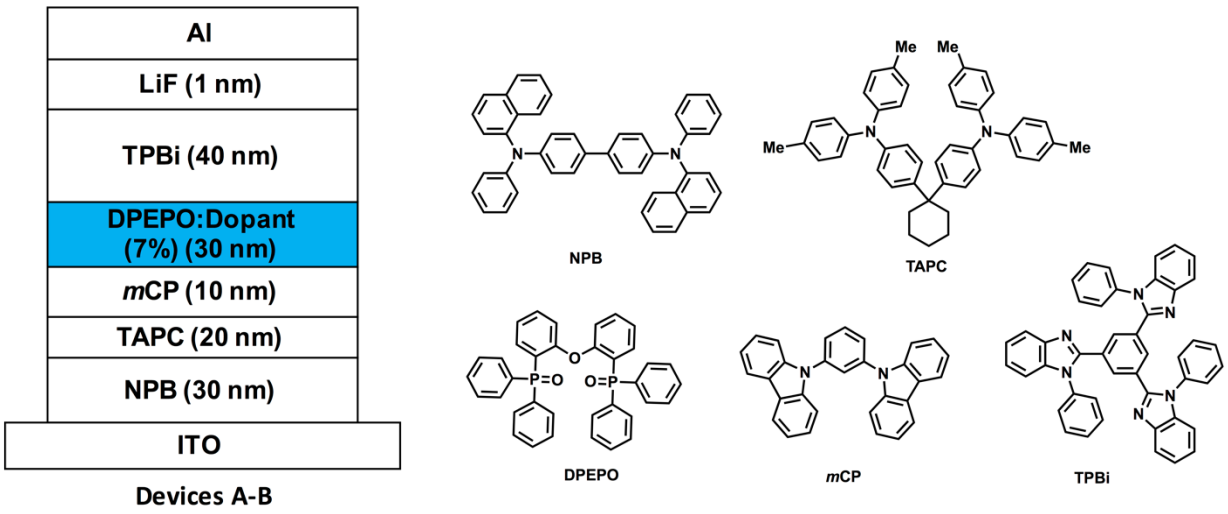

Fig. **5** Schematic representation of the devices A and B (left) and chemical structures of the materials used in the devices (right).

Devices A and B show maximum EQEs of 5.0% and 2.1%, respectively. Although, these emitters show slightly lower device performances compared to benzophenone-cored dicarbazole compound (EQE ~ 8.1%), device A shows a higher performance compared to the benzoyl pyridine and sulfone-based blue TADF devices (EQE ~ 2.2 - 4.1%).(18, 21, 23) The current efficiencies and power efficiencies for devices A and B are 7.3, 3.1 cd A^{-1}, and 4.2, 1.6 lm W^{-1}, respectively. The use of **3PyCzBP** (device A) as the dopant resulted in more than 2 times improvement of the EQE compared with **4PyCzBP** (device B) as the dopant. The higher EQE of device A can be correlated to the higher PL quantum yield of **3PyCzBP** as well as the more efficient up-conversion from the triplet to the singlet excited state as a function of the smaller ΔE_{ST}.

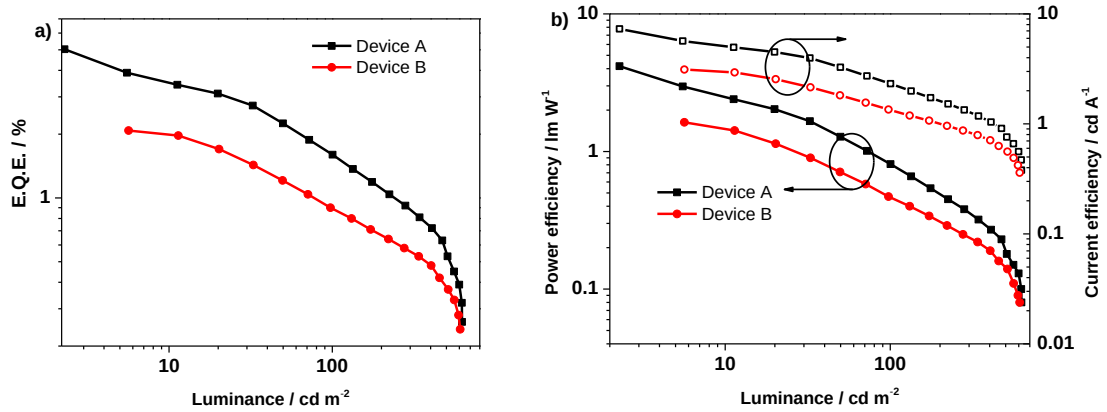

Fig. **6** Electroluminescent performance of devices A and B: a) EQE vs luminance, b) luminance vs current efficiency and power efficiency.

The electroluminescence spectra of both the devices are very similar to the corresponding thin film spectra, with no residual emission exhibited from other layers (Fig. **7**). This observation indicates that the excitons are confined within the emission layer without leakage to the adjacent layers. Both the devices A and B gave blue electroluminescence at the λ_{max} 457 nm and 450 nm

with color coordinates of (0.18, 0.21) and (0.19, 0.22), respectively. Although these devices do not possess deep blue color coordinates comparable to the boron-based compounds recently reported by Hatakeyama *et al*. (0.12, 0,13),(24) their CIE values are deeper than that reported for similar ketone-based TADF emitters (0.17, 0.38).(23)

Table **3.** The electroluminance performances of the device A and B

Device[a]	Dopant	V_d / V^b	L / cd m^{-2}, V	EQE / %, V	CE / cd A^{-1}, V	PE / lm W^{-1}, V	λ_{max} / nm	CIE / (x,y), 8V
A	**3PyCzBP**	5.5	663 (15.0)	5.0 (5.5)	7.3 (5.5)	4.2 (5.5)	457	0.18, 0.21
B	**4PyCzBP**	6.0	605 (14.5)	2.1 (6.0)	3.1 (6.0)	1.6 (6.0)	450	0.19, 0.22

[a]Device configuration for A and B: ITO/NPB (30 nm)/TAPC (20 nm)/*m*CP (10 nm)/DPEPO:**3PyCzBP** or **4PyCzBP** (7 wt%) (30 nm)/ TPBi (40 nm)/LiF (1 nm)/Al (100 nm); [b]V_d, The operating voltage at a brightness of 1 cd m^{-2}; L, maximum luminance; EQE, maximum external quantum efficiency; CE, maximum current efficiency; PE, maximum power efficiency; and λ_{max}, the wavelength where the EL spectrum has the highest intensity.

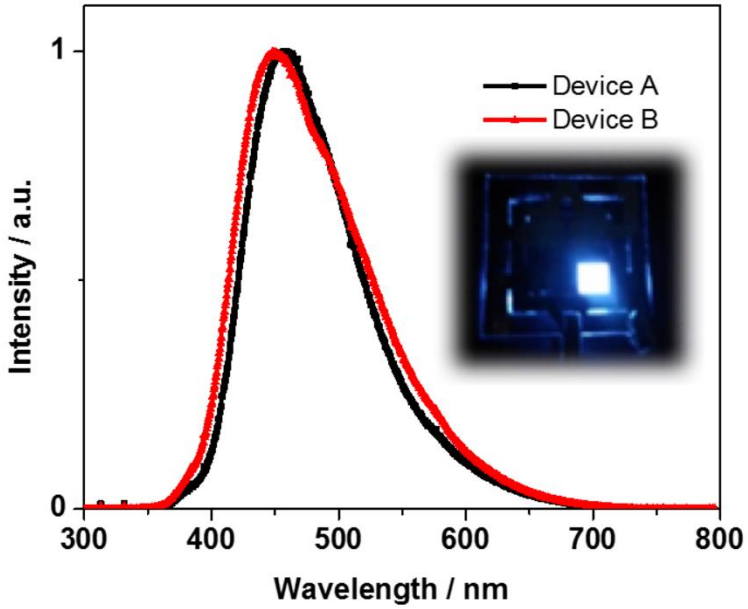

Fig. **7** Electroluminescence spectra of devices A and B measured at 10 V. The inset shows the photograph of device A.

Table **4.** The electroluminance performances of the device A and B at 100 cd m^{-2}.

Device[a]	Dopant	EQE / %	CE / cd A^{-1}	PE / lm W^{-1}
A	**3PyCzBP**	1.6	3.2	3.2
B	**4PyCzBP**	0.9	1.9	1.9

[a] EQE, maximum external quantum efficiency; CE, maximum current efficiency; and PE, maximum power efficiency.

OLED device performances at 100 cd m^{-2} are summarized in Table **4**. The EQE dropped from 5.0 to 1.6% for device A and from 2.1 to 0.9% for device B. Similarly, the current and power efficiency also dropped from 7.3 to 3.2 cd A^{-1}, 4.2 to 1.6 cd A^{-1} and 4.2 to 0.79 lm W^{-1}, 1.6 to 0.46 lm W^{-1}, respectively, for device A and B. High turn-on voltage (Table **3**) and significant roll-off (Table **4**) is observed in these devices due to non-ambipolar host materials (DPEPO).

Experimental section

General Synthetic Procedures

Commercial chemicals were used as supplied without further purification. All reactions were performed using standard Schlenk techniques under inert nitrogen atmosphere with dry solvents. Column chromatography was performed using silica gel (Silia-P from Silicycle, 60 Å, 40-63 μm). Analytical thin layer chromatography (TLC) was performed with silica plates with polymer (250 μm with indicator F-254) and compounds were visualized under UV light. ^{1}H and ^{13}C solution-phase NMR spectra were recorded on a Bruker Avance spectrometer operating at 11.7 T (Larmor frequencies of 500, 126 and 471 MHz, respectively). The following abbreviations have been used for multiplicity assignments: “s” for singlet, “d” for doublet, “t” for triplet, “m” for multiplet and “br” for broad. Melting points (Mps) were recorded using open-ended capillaries on an Electrothermal melting point apparatus and are uncorrected. High-resolution mass spectra of all compounds were recorded at the EPSRC UK National Mass Spectrometry Facility at

Swansea University on a quadrupole time-of-flight (ESI-Q-TOF), model ABSciex 5600 Triple TOF in positive electrospray or nanospray ionization mode and spectra were recorded using sodium formate solution as the calibrant.

Synthesis of 3,6-dibromo-9*H*-carbazole

The synthesis of this ligand is by a previously reported method.(25) 9H-carbazole (5.0 g, 0.03 mol, 1 equiv.) was added to a 50 mL round bottomed flask and dissolved with 10 mL of dry acetonitrile (MeCN). The mixture was cooled to a 0 °C with an ice bath and a solution of N-bromosuccinimide (NBS) (10.7 g, 0.06 mol, 2 equiv.) in 40 mL MeCN was added dropwise using a dropping funnel. The solution was slowly allowed to come to room temperature and stirred for an additional period of 2 hours. The mixture was poured onto distilled water and extracted multiple times with ethyl acetate. The organic fractions were combined, washed with a portion of brine and dried over magnesium sulfate. Filtration and evaporation under reduced pressure gave the desired product as a white solid. **Yield:** 87%. **Mp**: 209-212°C **^{1}H NMR (500 MHz, $CDCl_3$) δ (ppm):** 8.16 (d, *J* = 2.0 Hz, 2H, 7.55 (dd, *J* = 8.6, 1.9 Hz, 2H), 7.34 (d, *J* = 8.6 Hz, 2H). The characterization matches that reported.(26)

Synthesis of (4-(3,6-dibromo-9H-carbazol-9-yl)phenyl)(phenyl)methanone

3,6-dibromocarbazole (1.50 g, 4.61 mmol, 1 equiv.) and potassium *tert*-butoxide (0.52 g, 4.61 mmol, 1 equiv.) were added to a 50 mL round bottomed flask and dissolved in dry DMF (25 mL). The mixture was heat at 150 °C for 30 min and subsequently 4-fluorobenzophenone (0.92 g, 4.61 mmol, 1 equiv.) was added. The reaction mixture was degassed by multiple vacuum and N_2 purging cycles it was refluxed for 18 h under inert atmosphere. The reaction mixture was cooled down and poured in distilled water. The mixture was extracted multiple times with DCM, the organic fractions were combined, washed with a portion of brine and dried over magnesium

sulfate. Filtration and evaporation under reduced pressure gave the crude product (3.2 g). The crude product was purified by column chromatography (silica, dichloromethane) to give 0.90 g of pure compound as a white solid. **Yield**: 54%. **R_f**: 0.76 (DCM on silica). **Mp**: 226-228°C. **^{1}H NMR (500 MHz, $CDCl_3$) δ (ppm):** 8.24 (d, *J* = 1.8 Hz, 2H), 8.12 – 8.08 (m, 2H), 7.93 (dd, *J* = 8.7, 1.9 Hz, 2H), 7.71 – 7.65 (m, 3H), 7.60 – 7.55 (m, 4H), 7.39 (d, *J* = 8.7 Hz, 2H). **^{13}C NMR (500 MHz, $CDCl_3$) δ (ppm):** 195.45, 140.57, 139.29, 137.18, 136.73, 132.85, 132.06, 129.68, 128.53, 126.26, 124.38, 123.42, 113.71, 111.50 (Fig. **10, 11** (appendix)). **HR-MS: Calculated:** ($C_{25}H_{15}Br_2NO$): 505.9573, **Found:** 505.9565.

General syntheses of 3PyCzBP and 4PyCzBP

The (4-(3,6-dibromo-9H-carbazol-9-yl)phenyl)(phenyl)methanone (0.40 g, 0.79 mmol, 1.0 equiv.), 3-pyridinylboronic acid or 4-pyridinylboronic acid (0.24 g, 1.99 mmol, 2.5 equiv.) and cesium carbonate (1.55 g, 4.75 mmol, 6.0 equiv.) were added to a round-bottomed flask containing 50 mL of a mixture of 1,4-dioxane and distilled water (4:1 v/v). The reaction mixture was degassed by multiple vacuum and N_2 purging cycles, and $Pd(PPh_3)_4$ (0.91 g, 0.079 mmol, 0.1 equiv.) was added to the flask under positive nitrogen pressure. The mixture was refluxed under nitrogen atmosphere for 48 h and then cooled to room temperature. The mixture was poured into distilled water and extracted multiple times with DCM. The organic fractions were combined, washed with a portion of brine and dried over magnesium sulfate. Filtration and evaporation under reduced pressure gave the crude products (1.0 g). The crude products were purified by flash column chromatography (2.5% MeOH/DCM on silica) to give 0.3 g and 0.2 g, respectively for **3PyCzBP** and **4PyCzBP**, of pure compounds as white solids. Characterisation

of **3PyCzBP**. **Yield**: 60%. R_f = 0.45 (2.5% MeOH/DCM). **Mp:** 199-200°C. **^{1}H NMR (500 MHz, $CDCl_3$) δ (ppm):** 9.10 – 8.90 (m, 2H), 8.64 (dd, *J* = 4.8, 1.6 Hz, 2H), 8.44 (d, *J* = 1.6 Hz, 2H), 8.15 (d, *J* = 8.4 Hz, 2H), 8.09 – 8.02 (m, 2H), 7.98 – 7.91 (m, 2H), 7.81 (d, *J* = 8.4 Hz, 2H), 7.74 (dd, *J* = 8.6, 1.8 Hz, 2H), 7.70 – 7.65 (m, 3H), 7.59 (t, *J* = 7.6 Hz, 2H), 7.49 (s, 0H), 7.47 – 7.42 (m, 2H). **^{13}C NMR (500 MHz, $CDCl_3$) δ (ppm):** 195.40, 148.33, 147.97, 134.24, 131.91, 129.97, 128.44, 126.23, 125.86, 123.60, 119.08, 110.75 **HR-MS: Calculated:** ($C_{35}H_{24}N_3O$): 502.1914, **Found:** 502.1902 (Fig. **12-14**, (appendix)). CHN calculated for $C_{35}H_{23}N_3O \cdot 1/3\ CH_2Cl_2$: C, 80.09; H, 4.50; N, 7.93. Found: C, 80.05, H, 4.08; N, 8.24. Characterisation of **4PyCzBP**. **Yield**: 40%. R_f = 0.34 (2.5% MeOH/DCM). **Mp**: 200-202°C. **^{1}H NMR (500 MHz, $CDCl_3$) δ (ppm):** 8.74 – 8.70 (dd, 4H), 8.55 – 8.52 (d, *J* = 1.7 Hz, 2H), 8.18 – 8.13 (m, 2H), 7.98 – 7.93 (dd, 2H), 7.82 – 7.77 (m, 4H), 7.72 – 7.7 (m, 4H), 7.68-7.67 (t, 1H), 7.67-7.64 (2H, m), 7.62 – 7.57 (m, 2H). **^{13}C NMR (500 MHz, $CDCl_3$) δ (ppm):** 195.52, 150.25, 148.64, 141.30, 140.77, 137.20, 136.77, 132.88, 132.09, 131.17, 130.09, 128.56, 126.33, 125.84, 124.39, 121.72, 119.23, 110.79. **HR-MS: Calculated:** ($C_{35}H_{24}N_3O$): 502.1914, **Found:** 502.1902 (Fig. **15-17** (appendix)). CHN calculated for $C_{35}H_{23}N_3O \cdot 1/3\ CH_2Cl_2$: C, 80.09; H, 4.50; N, 7.93. Found: C, 79.92, H, 4.16; N, 8.12

Conclusion

We have designed two TADF emitters bearing a benzophenone core as the electron accepting unit and 3-pyridyl- and 4-pyridyl-decorated carbazole as the electron-donating unit. The photophysical properties were studied for these compounds in solution and thin film. A comparison of these materials shows that **3PyCzBP** compound shows the highest photoluminescence quantum yield and smallest ΔE_{ST}. The photoluminescence quantum yield reaches 23.4% in the PMMA film and the EQE of the blue-emitting OLED using **3PyCzBP** as

the dopant reached 5.0%. This molecular design opens up a new approach to the design blue TADF emitters for blue OLEDs.

Acknowledgments

We thank the Marie Skłodowska-Curie Individual Fellowship (MCIF, no 749557), the Leverhulme Trust (RPG-2016-047) and EPSRC (EP/P010482/1) for financial support. We thank the EPSRC UK National Mass Spectrometry Facility at Swansea University for analytical services.

Appendix

Optoelectronic Characterization

Photophysical measurements

All samples were prepared in HPLC grade CH_2Cl_2 or CH_3CN with varying concentrations on the order of 10^{-3} – 10^{-5} M. Absorption spectra were recorded at room temperature using a Shimadzu UV-1800 double beam spectrophotometer. Molar absorptivity determination was verified by linear least-squares fit of the values obtained from at least four independent solutions at varying concentrations with absorbance ranging from 6.05×10^{-5} to 2.07×10^{-5} M.

The sample solutions for the emission spectra were prepared in HPLC-grade DCM or CH_3CN and degassed *via* three freeze-pump-thaw cycles using a quartz cuvette designed in-house. Steady-state emission and excitation spectra and time-resolved emission spectra were

recorded at 298 K using an Edinburgh Instruments F980. All samples for steady-state measurements were excited at 360 nm using a xenon lamp, while samples for time-resolved measurements were excited at 378 nm using a PDL 800-D pulsed diode laser. Photoluminescence quantum yields were determined using the optically dilute method.(27) A stock solution with absorbance of *ca*. 0.5 was prepared and then four dilutions were prepared with dilution factors between 2 and 20 to obtain solutions with absorbances of *ca*. 0.095 0.065, 0.05 and 0.018, respectively. The Beer-Lambert law was found to be linear at the concentrations of these solutions. The emission spectra were then measured after the solutions were rigorously degassed *via* three freeze-pump-thaw cycles prior to spectrum acquisition. For each sample, linearity between absorption and emission intensity was verified through linear regression analysis and additional measurements were acquired until the Pearson regression factor (R^2) for the linear fit of the data set surpassed 0.9. Individual relative quantum yield values were calculated for each solution and the values reported represent the slope value. The equation $\Phi_s = \Phi_r(A_r/A_s)(I_s/I_r)(n_s/n_r)^2$ was used to calculate the relative quantum yield of each of the sample, where Φ_r is the absolute quantum yield of the reference, *n* is the refractive index of the solvent, *A* is the absorbance at the excitation wavelength, and *I* is the integrated area under the corrected emission curve. The subscripts *s* and *r* refer to the sample and reference, respectively. A solution of quinine sulfate in 0.5 M H_2SO_4 (Φ_r = 54.6%)(28) was used as external reference.(29)

PMMA-doped thin films were prepared by spin coating the samples from a solution of 2-methoxyethanol (HPLC grade) 10^{-2} M containing 10% w/w of the desired sample on a quartz substrate. Each sample was spin-coated three times from two different solutions following identical conditions and reproducible results were obtained. Steady-state emission and excitation spectra and time-resolved emission spectra of neat films were recorded at 298 K using an

Edinburgh Instruments F980. Solid-state PLQY measurements of thin films were performed in an integrating sphere under a nitrogen purge in a Hamamatsu C9920-02 luminescence measurement system.(30)

Table **5**. Temperature-dependent emission decays of **3PyCzBP** and **4PyCzBP**

	τ_e (ns)[a]			
	77 K[a]	150 K[b]	200 K[c]	300 K[b,d]
3PyCzBP	25.1 (0.82), 160.0 (0.01), 1573.2 (0.17)	27.6 (0.84), 243.1 (0.1), 3639.0 (0.05)	24.7 (0.81), 567.5 (0.02), 9513 (0.17)	28 (0.71), 546.5 (0.07), 12545 (0.22)
4PyCzBP	31.1 (0.9), 631.2 (0.1)	32.3 (0.84), 713 (0.5), 2864.0 (0.11)	34.5 (0.76), 713.4 (0.07), 5876.7 (0.15)	33.5 (0.75), 611.3 (0.05), 6320 (0.20)

[a] Measurements under vacuum on PMMA doped thin films (10 w/w % of compound) formed by spin-coating on a quartz substrate. Values in parentheses are pre-exponential weighting factor, in relative % intensity, of the emission decay kinetics (λ_{exc} = 378 nm).

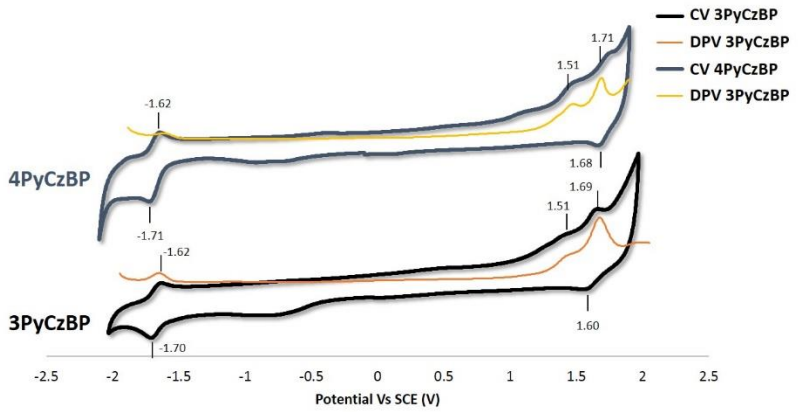

Fig. **8** Cyclic voltammogram (CV), black, and differential pulse voltammogram (DPV), yellow, of **3PyCzBP** and **4PyCzBP** in MeCN solution, reported versus SCE (Fc/Fc+ = 0.38 V in MeCN).

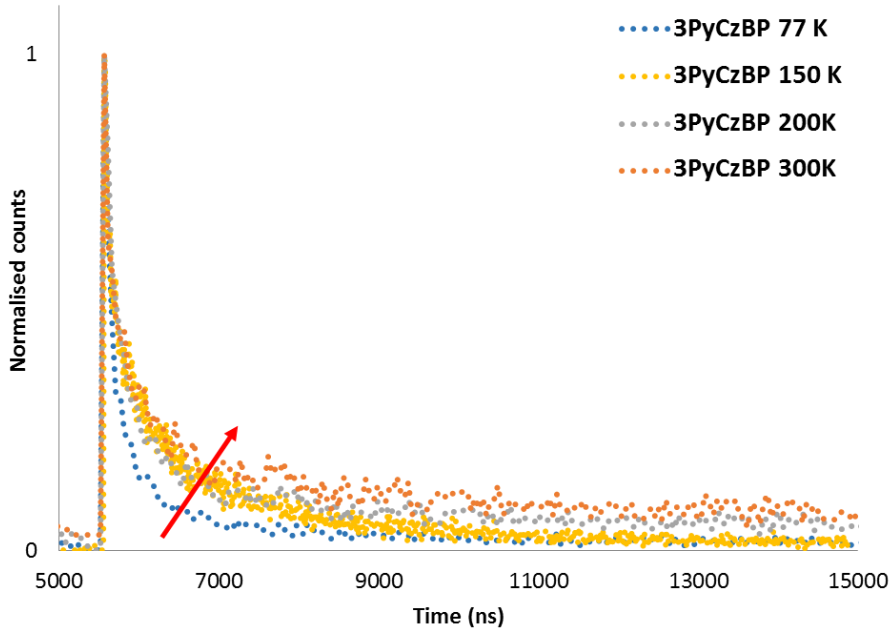

Fig. **9** Emission decay of **3PyCzBP** (λ_{exc} = 378 nm) collected on PMMA-doped thin film (10 w/w % of compound) formed by spin-coating deposition on quartz substrate at 77 K (in blue), at 150 K (in yellow), at 200 K (in grey) and at 300 K (in orange).

Characterization

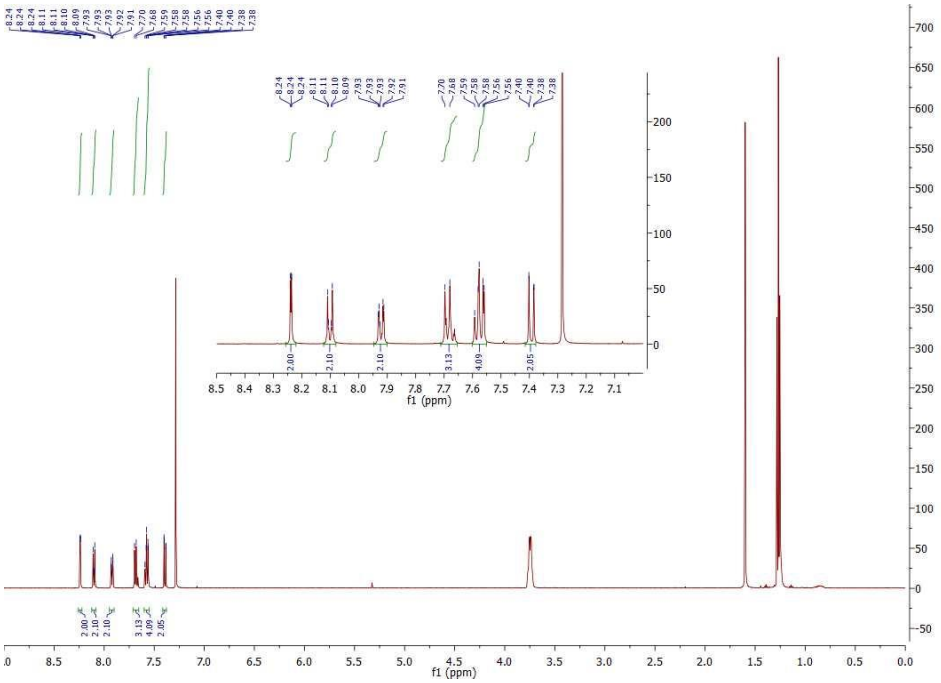

Fig. **10** ^{1}H NMR spectrum of (4-(3,6-dibromo-9H-carbazol-9-yl)phenyl)(phenyl)methanone in $CDCl_3$.

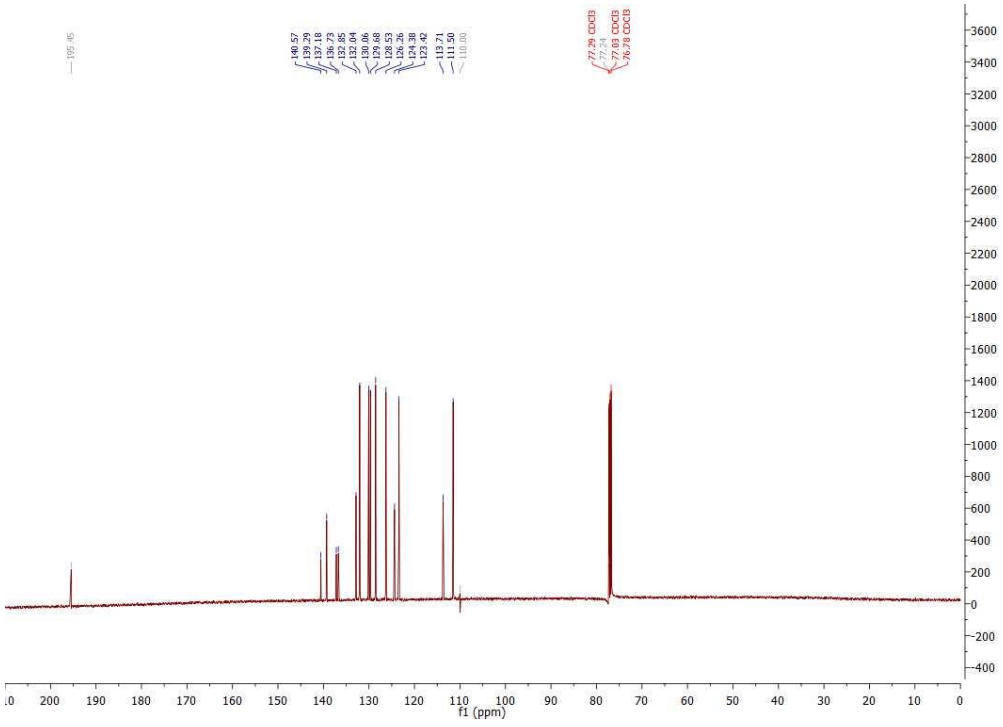

Fig. **11** ^{13}C NMR spectrum of (4-(3,6-dibromo-9*H*-carbazol-9-yl)phenyl)(phenyl)methanone in $CDCl_3$.

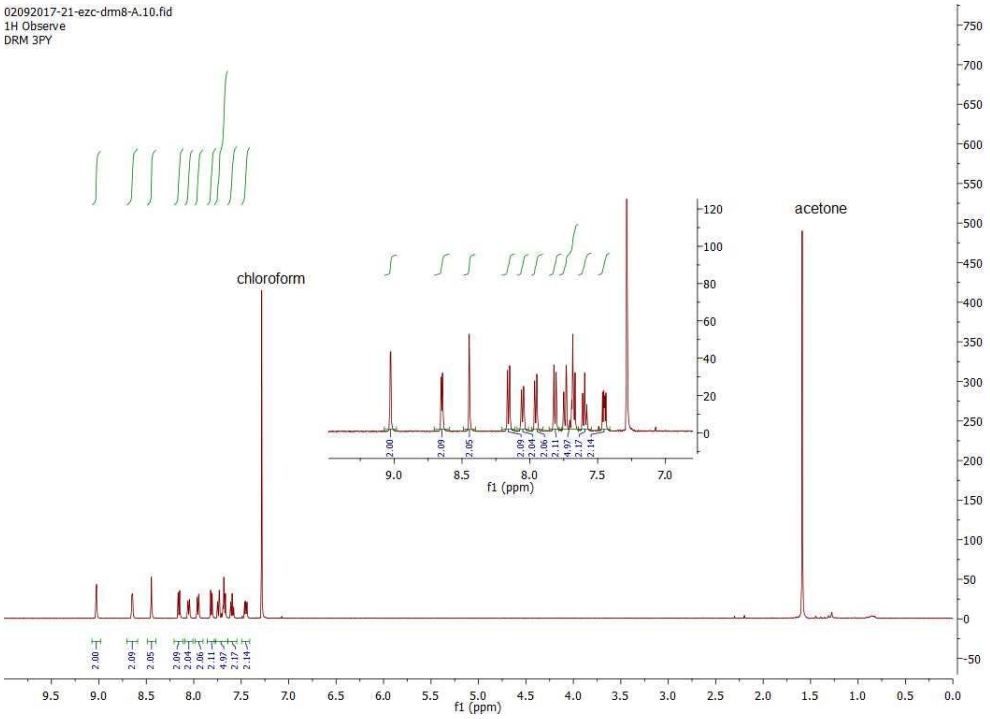

391

392 Fig. **12** ^{1}H NMR spectrum of **3PyCzBP** in $CDCl_3$.

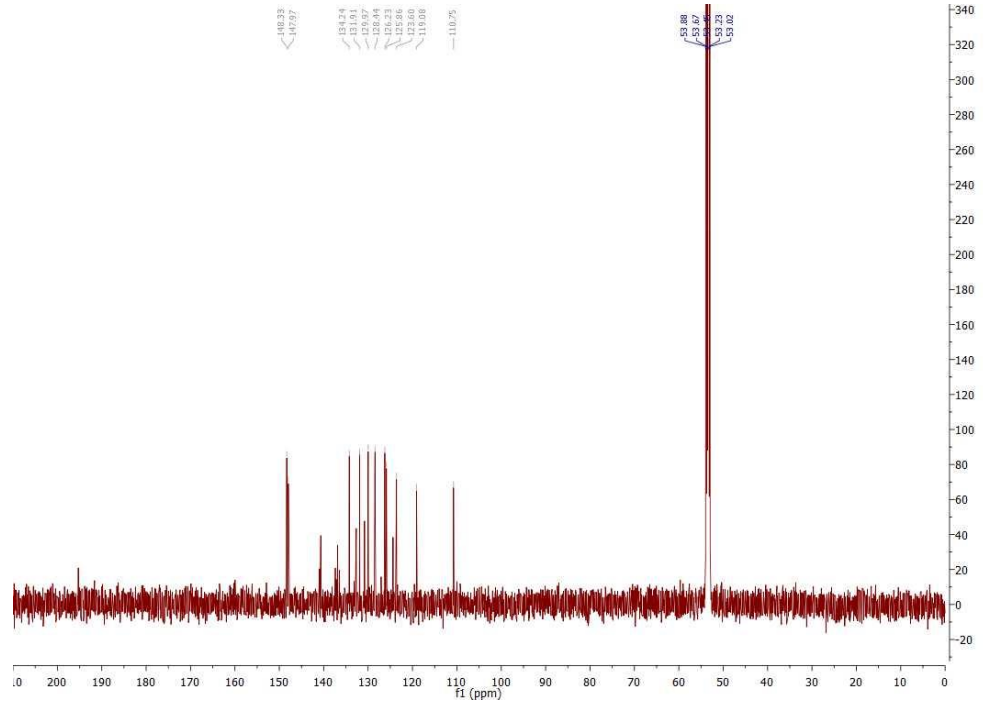

393

394 Fig. **13** ^{13}C NMR spectrum of **3PyCzBP** in $CDCl_3$.

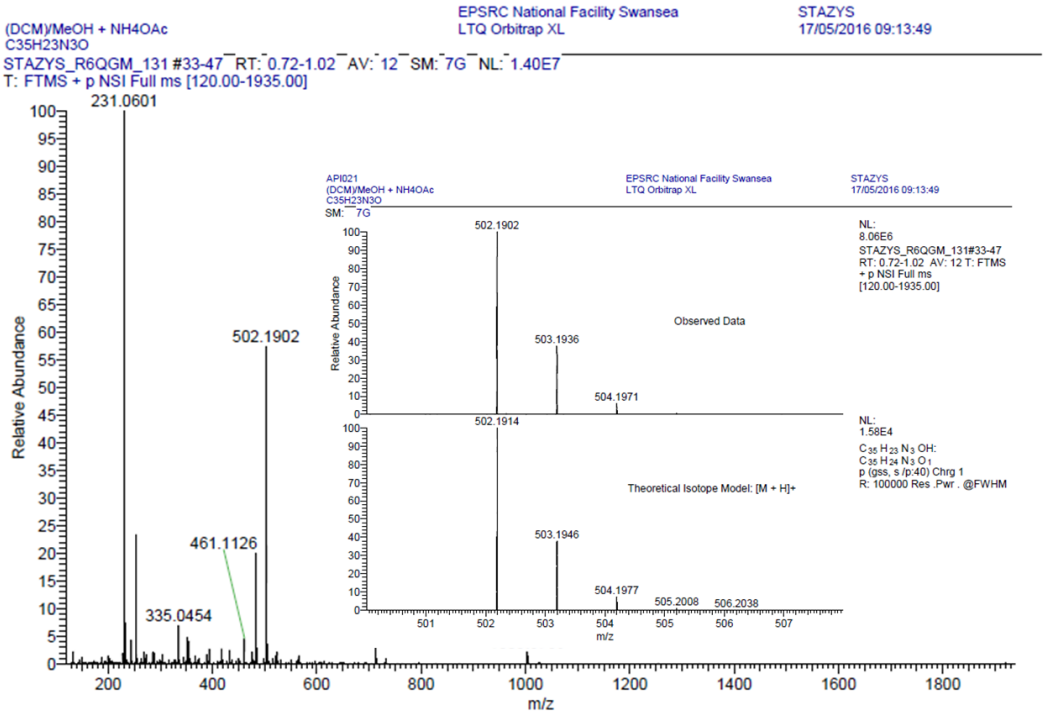

395

396 Fig. **14** HR-MS spectra of **3PyCzBP**.

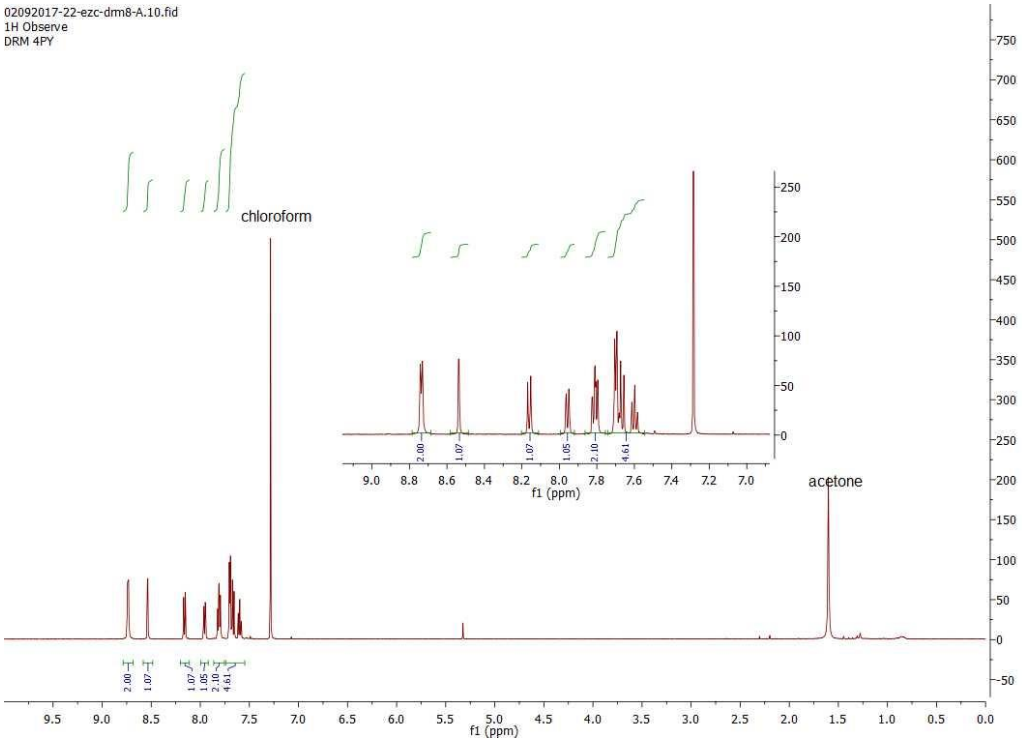

397

398 Fig. **15** ^{1}H NMR spectrum of **4PyCzBP** in $CDCl_3$.

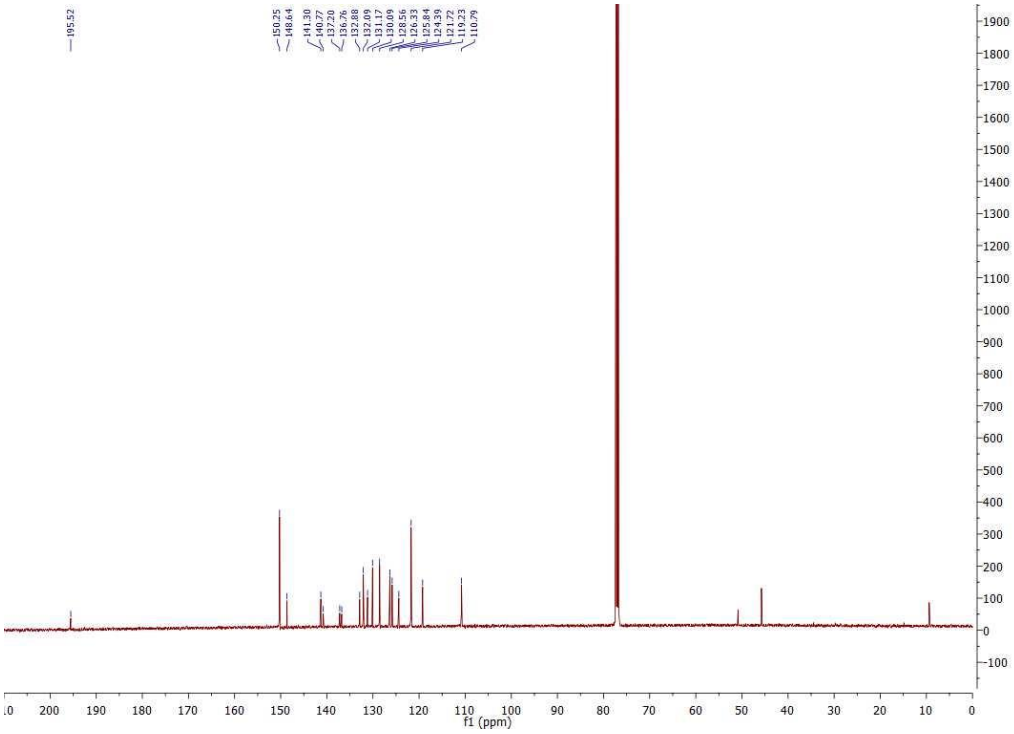

399

400 Fig. **16** ^{13}C NMR spectrum of **4PyCzBP** in $CDCl_3$.

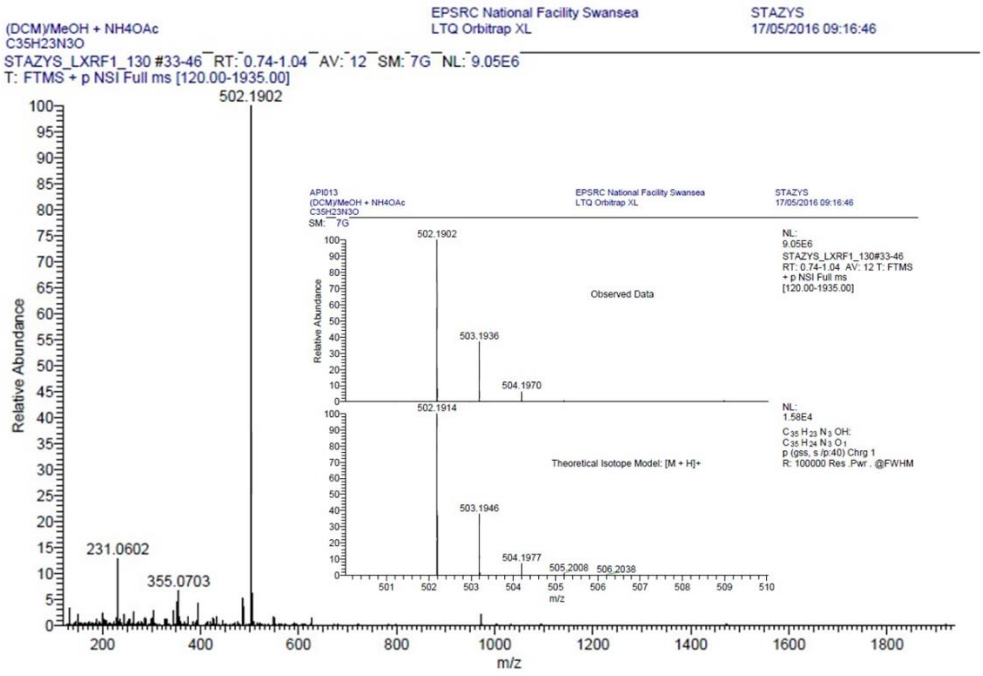

401

402 Fig. **17** HR-MS spectra of **4PyCzBP**.

DFT Calculations

The calculations were performed with the Gaussian 09,(31) revision D.018 suite of programs. Initially the geometries of **3PyCzBP** and **4PyCzBP** were fully optimized using a DFT methodology employing the PBE0(32) functional with the standard Pople(33) 6-31G(d,p) basis set and Tamm–Dancoff approximation (TDA) was treated as a variant of Time-dependent density functional theory (TD-DFT).(34) The molecular orbitals were visualized using GaussView 5.0 software.(35)

Table **6**. Main transitions and electron contour plots of molecular orbitals of **3PyCzBP**.

Transition (Wavelength)	Orbitals	Probabilities	Oscillator strength *(f)*	Character
$S_0 \rightarrow S_1$ (366 nm)	HOMO→LUMO	97%	0.31	3Pyrdine (3Py) and carbazole (Cz) to benzophenone (BP) (CT)
$S_0 \rightarrow S_5$ (293 nm)	HOMO-1→LUMO+1	13%	0.25	3PyCz to Cz (CT + (π- π*))
	HOMO→ LUMO+2	84%		3PyCz to 3PyCz (π- π*)
$S_0 \rightarrow S_8$ (271 nm)	HOMO-2→LUMO	37%	0.24	3PyCz to BP (CT + (π- π*))
	HOMO-1→LUMO+1	31%		3PyCz to Cz (CT + (π- π*))

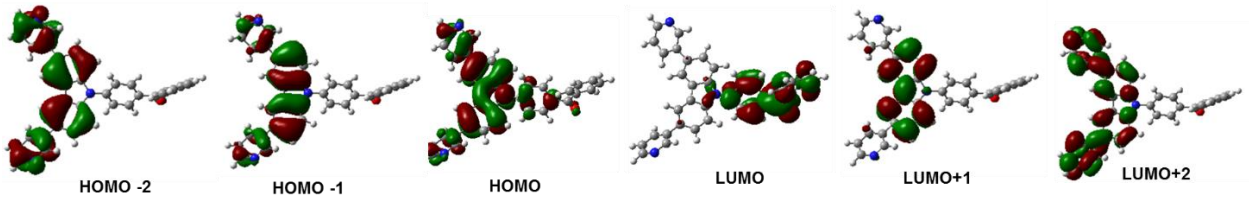

Table **7**. Main transitions and electron contour plots of molecular orbitals of **4PyCzBP**.

Transition (Wavelength)	Orbitals	Probabilities	Oscillator strength *(f)*	Character
$S_0 \rightarrow S_1$ (359 nm)	HOMO→LUMO	97%	0.33	4Pyrdine (4Py) and carbazole (Cz) to

				benzophenone (BP) (CT)
$S_0 \rightarrow S_4$ (297 nm)	HOMO-1→LUMO+1	11%	0.29	4PyCz to Cz (π-π* + CT)
	HOMO→LUMO+2	86%		4PyCz to 4PyCz (π-π*)
$S_0 \rightarrow S_7$ (266 nm)	HOMO-2→LUMO	12%	0.45	4PyCz to BP (CT)
	HOMO-1 → LUMO+1	40%		4PyCz to Cz (π-π* + CT)
	HOMO-1 → LUMO+3	16%		4PyCz to BP (CT+ π-π*)

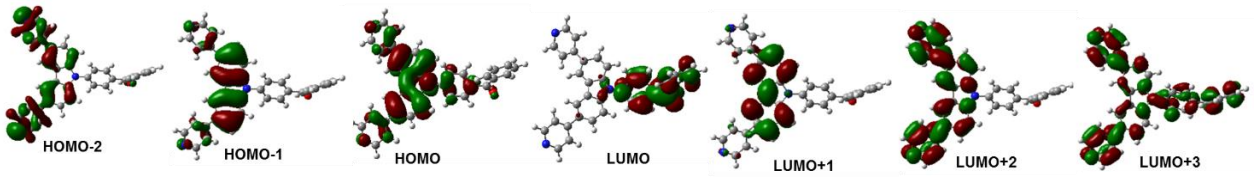

Table **8**. Main transitions and electron contour plots of molecular orbitals of **CzBP**.

Transition (Wavelength)	Orbitals	Probabilities	Oscillator strength *(f)*	Character
$S_0 \rightarrow S_1$ (361)	HOMO→LUMO	97%	0.26	Carbazole (Cz) to benzophenone (BP) (CT)

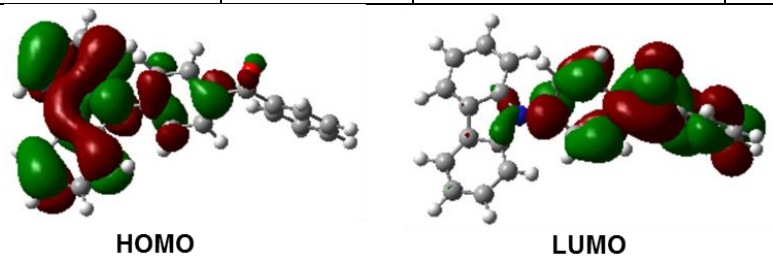

Table **9**. Main transitions and electron contour plots of molecular orbitals of **PyCz**.

Transition (Wavelength)	Orbitals	Probabilities	Oscillator strength *(f)*	Character
$S_0 \rightarrow S_2$ (293 nm)	HOMO-1→LUMO	14%	0.28	Pyrdine carbazole (PyCz) to Pyrdine carbazole (PyCz) (π-π*)
	HOMO→LUMO+1	83%		PyCz to PyCz (π-π*)
$S_0 \rightarrow S_4$ (264 nm)	HOMO-1→LUMO	50%	0.85	PyCz to PyCz (π-π*)
	HOMO-1→LUMO+2	26%		PyCz to PyCz (π-π*)
	HOMO→LUMO+1	10%		PyCz to PyCz (π-π*)
$S_0 \rightarrow S_7$	HOMO-	56%	0.45	PyCz to PyCz (π-π*)

(247 nm)	1→LUMO+1			
	HOMO → LUMO+2	23%		PyCz to PyCz (π-π*)
$S_0 \rightarrow S_{10}$ (239 nm)	HOMO-1→LUMO	19%	0.45	PyCz to PyCz (π-π*)
	HOMO-1→LUMO+2	59%		PyCz to PyCz (π-π*)
	HOMO→LUMO+5	10%		PyCz to PyCz (π-π*)

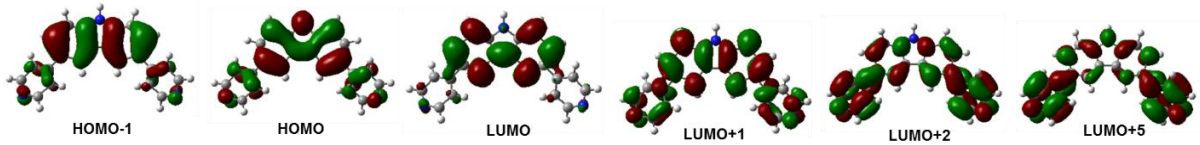

Table **10**. Optimized Atomic coordinates of **3PyCzBP** obtained from DFT calculations.

Center Number	Atomic Number	Atomic Type	Coordinates (Angstroms) X	Y	Z
1	6	0	8.370275	0.517539	-0.149998
2	6	0	7.410758	-0.283577	-0.768893
3	6	0	6.351926	-0.804268	-0.024977
4	6	0	6.252753	-0.523914	1.337765
5	6	0	7.212301	0.277109	1.956677
6	6	0	8.271101	0.797893	1.212745
7	6	0	3.121177	-2.074858	-1.146026
8	6	0	1.768527	-1.751968	-1.038469
9	6	0	1.375510	-0.627885	-0.312089
10	6	0	2.335135	0.173138	0.306768
11	6	0	3.687758	-0.149792	0.199299
12	6	0	4.080801	-1.273834	-0.527169
13	6	0	5.409376	-1.591045	-0.632827
14	8	0	5.749755	-2.564490	-1.261964

441	15	7	0	0.134221	-0.331457	-0.213441
442	16	6	0	-0.359965	0.951518	-0.193917
443	17	6	0	-1.745846	0.853110	-0.076595
444	18	6	0	-2.074374	-0.539606	-0.025535
445	19	6	0	-0.880257	-1.254141	-0.113068
446	20	6	0	-3.282256	-1.259160	0.087535
447	21	6	0	-3.251264	-2.658374	0.108660
448	22	6	0	-2.041321	-3.342592	0.019156
449	23	6	0	-0.830299	-2.653216	-0.093570
450	24	6	0	0.309538	2.178753	-0.270682
451	25	6	0	-0.464467	3.342145	-0.225914
452	26	6	0	-1.850934	3.277920	-0.109109
453	27	6	0	-2.503580	2.041970	-0.033595
454	28	6	0	-4.413401	-3.356350	0.217596
455	29	6	0	-2.577405	4.426900	-0.068044
456	30	6	0	-3.924143	4.432935	-0.415899
457	31	6	0	-4.636131	5.626750	-0.362135
458	32	6	0	-3.966878	6.771682	0.039848
459	33	7	0	-2.660658	6.796982	0.383500
460	34	6	0	-1.995616	5.622786	0.321471
461	35	6	0	-4.414345	-4.673509	0.648238
462	36	7	0	-5.532192	-5.420867	0.777939
463	37	6	0	-6.700939	-4.821649	0.461973

464	38	6	0	-6.801432	-3.511083	0.023041
465	39	6	0	-5.632695	-2.767051	-0.100304
466	40	1	0	9.205234	0.928251	-0.736648
467	41	1	0	7.489044	-0.504740	-1.843583
468	42	1	0	5.417751	-0.934566	1.924396
469	43	1	0	7.134090	0.498142	3.031399
470	44	1	0	9.027849	1.429673	1.700788
471	45	1	0	3.431149	-2.961257	-1.718927
472	46	1	0	1.011744	-2.383753	-1.526451
473	47	1	0	2.025165	1.059578	0.879605
474	48	1	0	4.444524	0.481914	0.687410
475	49	1	0	-4.241149	-0.724857	0.158562
476	50	1	0	-2.038604	-4.442437	0.037452
477	51	1	0	0.126971	-3.190450	-0.164370
478	52	1	0	1.404656	2.225874	-0.362858
479	53	1	0	0.029154	4.323461	-0.283836
480	54	1	0	-3.598838	1.998193	0.058561
481	55	1	0	-4.421029	3.503269	-0.730261
482	56	1	0	-5.702077	5.661046	-0.631550
483	57	1	0	-4.531978	7.714511	0.081523
484	58	1	0	-0.930471	5.615508	0.596086
485	59	1	0	-3.448960	-5.137360	0.898982
486	60	1	0	-7.626564	-5.408043	0.558714

487	61	1	0	-7.779445	-3.070888	-0.221328
488	62	1	0	-5.672203	-1.723422	-0.445670

489

490 Table **11**. Optimized Atomic coordinates of **4PyCzBP** obtained from DFT calculations.

Center Number	Atomic Number	Atomic Type	Coordinates (Angstroms) X	Y	Z
1	6	0	8.935797	0.176230	0.173023
2	6	0	7.921793	-0.486484	-0.417081
3	6	0	6.637730	-0.383452	0.018998
4	6	0	6.453030	0.362537	1.123804
5	6	0	7.460057	1.029058	1.725814
6	6	0	8.706723	0.947419	1.242279
7	6	0	3.390065	-1.745322	-0.900608
8	6	0	2.066084	-1.543286	-0.793193
9	6	0	1.498594	-0.416507	-0.314076
10	6	0	2.427113	0.501328	0.026500
11	6	0	3.755472	0.314597	-0.060108
12	6	0	4.298261	-0.835756	-0.496983
13	6	0	5.644122	-1.085555	-0.621801
14	8	0	5.980451	-1.998454	-1.357066
15	6	0	-0.431329	0.888225	-0.201751
16	6	0	-1.743346	0.701348	-0.089552
17	6	0	-1.927017	-0.620108	-0.050930

511	18	6	0	-0.694697	-1.153186	-0.124173
512	19	7	0	0.214593	-0.235533	-0.221390
513	20	6	0	-3.065213	-1.338990	0.050153
514	21	6	0	-3.047909	-2.682516	0.118077
515	22	6	0	-1.807569	-3.215292	0.119050
516	23	6	0	-0.668143	-2.481151	0.019789
517	24	6	0	-0.076859	2.180408	-0.369580
518	25	6	0	-0.972513	3.172596	-0.317894
519	26	6	0	-2.306826	2.990200	-0.130395
520	27	6	0	-2.665789	1.698668	-0.038026
521	28	6	0	-4.178483	-3.433765	0.211789
522	29	6	0	-3.202193	4.013179	-0.074174
523	30	6	0	-4.180235	-4.777507	0.282360
524	31	6	0	-5.339210	-5.483215	0.373758
525	32	7	0	-6.481592	-4.956465	0.398843
526	33	6	0	-6.520639	-3.695957	0.331124
527	34	6	0	-5.442689	-2.907181	0.238566
528	35	6	0	-2.856576	5.315258	-0.167360
529	36	6	0	-3.783416	6.294807	-0.104497
530	37	7	0	-5.018979	6.090106	0.043405
531	38	6	0	-5.377231	4.882697	0.137234
532	39	6	0	-4.533291	3.838458	0.086892
533	40	1	0	9.961741	0.083047	-0.222422

534	41	1	0	8.202593	-1.091850	-1.295642
535	42	1	0	5.492434	0.412272	1.656727
536	43	1	0	7.269750	1.616658	2.640396
537	44	1	0	9.535576	1.480993	1.736036
538	45	1	0	3.693608	-2.712863	-1.337043
539	46	1	0	1.462479	-2.350366	-1.230163
540	47	1	0	2.152048	1.462078	0.479845
541	48	1	0	4.365563	1.192703	0.198393
542	49	1	0	-3.997451	-0.763055	0.080033
543	50	1	0	-1.633217	-4.295839	0.233281
544	51	1	0	0.262620	-3.055679	0.121676
545	52	1	0	0.946583	2.495660	-0.611742
546	53	1	0	-0.539073	4.172127	-0.473200
547	54	1	0	-3.710784	1.387842	0.076382
548	55	1	0	-3.268524	-5.391546	0.268870
549	56	1	0	-5.314500	-6.585563	0.430294
550	57	1	0	-7.529517	-3.247901	0.352007
551	58	1	0	-5.658458	-1.830402	0.187826
552	59	1	0	-1.823504	5.668663	-0.294994
553	60	1	0	-3.478767	7.353129	-0.182747
554	61	1	0	-6.460608	4.715112	0.268430
555	62	1	0	-5.014377	2.854964	0.186099

556 Table **12**. Optimized Atomic coordinates of **CzBP** obtained from DFT calculations.

Center Number	Atomic Number	Atomic Type	Coordinates (Angstroms) X	Y	Z
1	6	0	-6.806531	5.381945	0.549127
2	6	0	-7.240051	6.204869	1.527717
3	6	0	-7.620160	5.666917	2.690682
4	6	0	-7.548093	4.339833	2.882538
5	6	0	-7.071003	3.494632	1.940694
6	6	0	-6.739447	4.060500	0.760709
7	6	0	-5.237999	1.526821	0.683593
8	6	0	-6.289332	1.232183	1.477562
9	6	0	-6.533457	-0.087429	1.588786
10	6	0	-5.838582	-1.016002	0.899228
11	6	0	-4.814741	-0.740997	0.063747
12	6	0	-4.549622	0.580035	0.015038
13	7	0	-4.152251	-1.649217	-0.589125
14	6	0	-2.936987	-1.569768	-1.029736
15	6	0	-2.582871	-2.699325	-1.666962
16	6	0	-3.636085	-3.507321	-1.593689
17	6	0	-4.581436	-2.823261	-0.934923
18	6	0	-1.953167	-0.657879	-0.894929
19	6	0	-0.740523	-0.835580	-1.454214
20	6	0	-0.448708	-1.955693	-2.141214
21	6	0	-1.384677	-2.923727	-2.238016

581	22	6	0	-3.777958	-4.755151	-2.077537
582	23	6	0	-4.971007	-5.360330	-1.919870
583	24	6	0	-5.971933	-4.683105	-1.323149
584	25	6	0	-5.783265	-3.431584	-0.858587
585	26	6	0	-7.024622	2.144321	2.196352
586	27	8	0	-7.684406	1.722791	3.131292
587	28	1	0	-6.542678	5.804246	-0.435772
588	29	1	0	-7.308895	7.292158	1.358785
589	30	1	0	-7.997240	6.324386	3.492679
590	31	1	0	-7.877230	3.991443	3.876267
591	32	1	0	-6.473369	3.473088	-0.129998
592	33	1	0	-4.845079	2.549037	0.579770
593	34	1	0	-7.326267	-0.476091	2.251473
594	35	1	0	-6.112219	-2.048956	1.154959
595	36	1	0	-3.780855	0.992130	-0.651258
596	37	1	0	-2.039466	0.252338	-0.288040
597	38	1	0	0.044957	-0.070941	-1.323956
598	39	1	0	0.551416	-2.101477	-2.581962
599	40	1	0	-1.148361	-3.864256	-2.759351
600	41	1	0	-2.964171	-5.278697	-2.602782
601	42	1	0	-5.137262	-6.377113	-2.312620
602	43	1	0	-6.966857	-5.155490	-1.248822
603	44	1	0	-6.692029	-2.949819	-0.474342

Table **13**. Optimized Atomic coordinates of **PyCz** obtained from DFT calculations.

Center Number	Atomic Number	Atomic Type	Coordinates (Angstroms) X	Y	Z
1	6	0	-1.132907	3.309931	0.989010
2	6	0	-0.655795	2.169817	0.300516
3	6	0	-1.541423	1.103501	0.094593
4	6	0	-2.853511	1.174308	0.559164
5	6	0	-3.296282	2.336435	1.246672
6	6	0	-2.432505	3.411854	1.464012
7	6	0	-3.982869	0.273862	0.510661
8	6	0	-5.052507	0.936126	1.171461
9	7	0	-4.609907	2.161577	1.597299
10	6	0	-4.180125	-1.000204	-0.018671
11	6	0	-5.425483	-1.632713	0.096045
12	6	0	-6.466094	-0.942018	0.760600
13	6	0	-6.302345	0.326423	1.298302
14	6	0	-5.648513	-2.975639	-0.457018
15	6	0	0.730677	2.109039	-0.183751
16	6	0	-6.885930	-3.632467	-0.359667
17	6	0	-7.041952	-4.905564	-0.902121
18	7	0	-6.079167	-5.580511	-1.530631

627	19	6	0	-4.902484	-4.961028	-1.625583
628	20	6	0	-4.638163	-3.690840	-1.119746
629	21	6	0	1.641746	3.159489	0.009832
630	22	6	0	2.945038	3.047571	-0.471015
631	23	7	0	3.418342	1.988699	-1.123482
632	24	6	0	2.557867	0.989035	-1.309855
633	25	6	0	1.235334	0.995131	-0.872404
634	26	1	0	-0.466605	4.144756	1.158857
635	27	1	0	-1.215297	0.212218	-0.427952
636	28	1	0	-2.753132	4.304059	1.985469
637	29	1	0	-5.162088	2.827647	2.089560
638	30	1	0	-3.357373	-1.495129	-0.520503
639	31	1	0	-7.435207	-1.411655	0.860665
640	32	1	0	-7.127344	0.816445	1.798297
641	33	1	0	-7.731589	-3.169727	0.131466
642	34	1	0	-8.004436	-5.399414	-0.818514
643	35	1	0	-4.110573	-5.500169	-2.135007
644	36	1	0	-3.647365	-3.275355	-1.248869
645	37	1	0	1.355809	4.064480	0.528795
646	38	1	0	3.635920	3.869143	-0.312434
647	39	1	0	2.932000	0.120000	-1.840713
648	40	1	0	0.616746	0.130765	-1.075073

649

650

References

1. Y. Im et al., "Recent Progress in High-Efficiency Blue-Light-Emitting Materials for Organic Light-Emitting Diodes," *Adv. Funct. Mater.* **27**(13), (2017).
2. S. E. Root et al., "Mechanical Properties of Organic Semiconductors for Stretchable, Highly Flexible, and Mechanically Robust Electronics," *Chem Rev* **117**(9), 6467-6499 (2017).
3. C. W. Tang, and S. A. VanSlyke, "Organic electroluminescent diodes," *Appl. Phys. Lett.* **51**(12), 913-915 (1987).
4. H. Yersin, *Highly Efficient OLEDs with Phosphorescent Materials*, Wiley-VCH, Weinheim (2008).
5. H. Wu et al., "Progress and perspective of polymer white light-emitting devices and materials," *Chem Soc Rev* **38**(12), 3391-3400 (2009).
6. H. Xu et al., "Recent progress in metal-organic complexes for optoelectronic applications," *Chem. Soc. Rev.* **43**(10), 3259-3302 (2014).
7. Y. Zhang, J. Lee, and S. R. Forrest, "Tenfold increase in the lifetime of blue phosphorescent organic light-emitting diodes," *Nat Commun* **5**(5008 (2014).
8. J. Lee et al., "Deep blue phosphorescent organic light-emitting diodes with very high brightness and efficiency," *Nat Mater* **15**(1), 92-98 (2016).
9. X. Yang, X. Xu, and G. Zhou, "Recent advances of the emitters for high performance deep-blue organic light-emitting diodes," *J. Mater. Chem. C* **3**(5), 913-944 (2015).
10. J. Zhou et al., "Upconversion luminescent materials: advances and applications," *Chem Rev* **115**(1), 395-465 (2015).
11. Y. Luo, and H. Aziz, "Correlation Between Triplet-Triplet Annihilation and Electroluminescence Efficiency in Doped Fluorescent Organic Light-Emitting Devices," *Adv. Funct. Mater.* **20**(8), 1285-1293 (2010).
12. C. Adachi, "Third-generation organic electroluminescence materials†," *Jpn. J. Appl. Phys.* **53**(6), 060101 (2014).
13. H. Uoyama et al., "Highly efficient organic light-emitting diodes from delayed fluorescence," *Nature* **492**(7428), 234-238 (2012).
14. M. Y. Wong, and E. Zysman-Colman, "Purely Organic Thermally Activated Delayed Fluorescence Materials for Organic Light-Emitting Diodes," *Adv Mater* **29**(1605444 (2017).
15. Z. Yang et al., "Recent advances in organic thermally activated delayed fluorescence materials," *Chem. Soc. Rev.* **46**(3), 915-1016 (2017).
16. Y. Im et al., "Molecular Design Strategy of Organic Thermally Activated Delayed Fluorescence Emitters," *Chem. Mater.* **29**(5), 1946-1963 (2017).
17. Y. J. Cho et al., "The design of dual emitting cores for green thermally activated delayed fluorescent materials," *Angew Chem Int Ed Engl* **54**(17), 5201-5204 (2015).
18. P. Rajamalli et al., "A Method for Reducing the Singlet-Triplet Energy Gaps of TADF Materials for Improving the Blue OLED Efficiency," *ACS Appl Mater Interfaces* **8**(40), 27026-27034 (2016).
19. D. R. Lee et al., "Design Strategy for 25% External Quantum Efficiency in Green and Blue Thermally Activated Delayed Fluorescent Devices," *Adv Mater* **27**(39), 5861-5867 (2015).
20. S. Hirata et al., "Highly efficient blue electroluminescence based on thermally activated delayed fluorescence," *Nat Mater* **14**(330-336 (2015).
21. S. Y. Lee et al., "Luminous butterflies: efficient exciton harvesting by benzophenone derivatives for full-color delayed fluorescence OLEDs," *Angew Chem Int Ed Engl* **53**(25), 6402-6406 (2014).
22. P. Rajamalli et al., "A thermally activated delayed blue fluorescent emitter with reversible externally tunable emission," *J. Mater. Chem. C* **4**(5), 900-904 (2016).

23. P. Rajamalli et al., "Thermally activated delayed fluorescence emitters with a m,m-di-tert-butyl-carbazolyl benzoylpyridine core achieving extremely high blue electroluminescence efficiencies," *J. Mater. Chem. C* **5**(11), 2919-2926 (2017).
24. T. Hatakeyama et al., "Ultrapure Blue Thermally Activated Delayed Fluorescence Molecules: Efficient HOMO–LUMO Separation by the Multiple Resonance Effect," *Adv. Mater.* **28**(14), 2777-2781 (2016).
25. E. Zysman-Colman, K. Arias, and J. S. Siegel, "Synthesis of Arylbromides from Arenes and NBS in Acetonitrile: A Convenient method for Aromatic Bromination," *Can. J. Chem.* **87**(2), 440-447 (2009).
26. A. Rembiak, and A. M. P. Koskinen, "Versatile Synthesis of Symmetrical Carbazole-Based Ligand Precursors- via Regioselective Aromatic Bromination," *Synthesis* **47**(21), 3347-3353 (2015).
27. G. A. Crosby, and J. N. Demas, "Measurement of photoluminescence quantum yields. Review," *J. Phys. Chem.* **75**(8), 991-1024 (1971).
28. W. H. Melhuish, "Quantum Efficiences Of Fluorescence Of Organic Substances: Effect Of Solvent And Concentration Of The Fluorescent Solute 1," *J. Phys. Chem.* **65**(2), 229-235 (1961).
29. A. M. Brouwer, "Standards for photoluminescence quantum yield measurements in solution (IUPAC Technical Report)*," *Pure Appl. Chem.* **83**(12), 2213-2228 (2011).
30. N. C. Greenham et al., "Measurement of absolute photoluminescence quantum efficiencies in conjugated polymers," *Chem. Phys. Lett.* **241**(1–2), 89-96 (1995).
31. M. J. Frisch et al., "Gaussian 09, Revision D.01," Gaussian Inc., Wallingford, CT (2013).
32. C. Adamo, and V. Barone, "Toward reliable density functional methods without adjustable parameters: The PBE0 model," *J. Chem. Phys.* **110**(13), 6158-6170 (1999).
33. J. A. Pople, J. S. Binkley, and R. Seeger, "Theoretical Models Incorporating Electron Correlation," *Int. J. Quant. Chem. Symp.* **10**(1 (1976).
34. M. Moral et al., "Theoretical Rationalization of the Singlet–Triplet Gap in OLEDs Materials: Impact of Charge-Transfer Character," *J. Chem. Theory Comput.* **11**(1), 168-177 (2015).
35. Dennington Roy, Keith Todd A., and Millam John M., "Gaussview," in *Gaussview ver 5.0*, Semichem, Inc., Shawnee Mission, KS (2009).

First Author P. Rajamalli is a Marie Curie Fellow at the University of St Andrews, working in the laboratory of Dr Eli Zysman-Colman. She received her BSc and MSc degrees in chemistry from the University of Madras 2005 and Bharathiar University 2007, respectively, and her PhD degree in chemistry from the Indian Institute of Technology Madras in 2012. She is the author of more than 23 journal papers and has filed three patents. Her current research interests include dendrimers, OLEDs and TADF emitters.

Second Author Diego Rota Martir obtained his BSc and MSc degrees in chemical science at the University of Milano-Bicocca in 2011 and 2013, respectively. After working at *Istituto Italiano di Tecnologia*@NEST in Pisa on nanoparticles, he started his PhD in 2014 at the University of St Andrews with Dr Eli Zysman-Colman working on the self-assembly of photoactive materials.

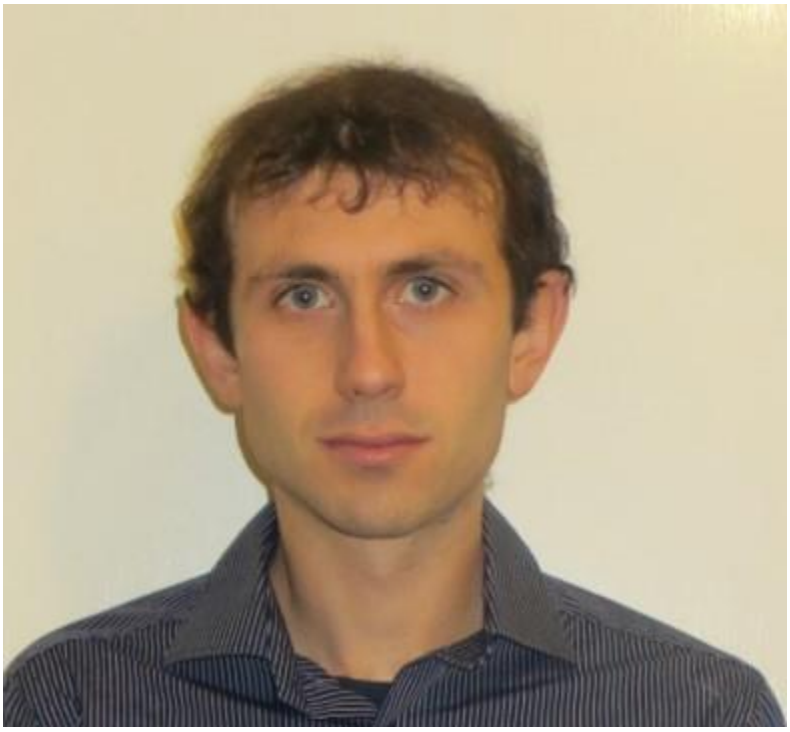

Last Author Eli Zysman-Colman obtained his Ph.D. from McGill University in 2003 under the supervision of Prof. David N. Harpp as an FCAR scholar where he conducting research in physical organic sulfur chemistry. He then completed two postdoctoral fellowships, one in supramolecular chemistry with Jay Siegel at the Organic Chemistry Institute, University of Zurich as an FQRNT fellow and the other in inorganic materials chemistry with Stefan Bernhard

at Princeton University as a PCCM fellow. He joined the department of chemistry at the Université de Sherbrooke in Quebec, Canada as an assistant professor in 2007. In 2013, he moved to the University of St Andrews where he is presently Reader in Optoelectronic Materials and Fellow of the Royal Society of Chemistry. His research program focuses on the rational design of: (I) luminophores for energy-efficient visual displays and flat panel lighting based on organic light emitting diode (OLED) and light-emitting electrochemical cell (LEEC) device architectures; (II) light harvesting dyes for dye-sensitized solar cells (DSSCs) and organic photovoltaics; (III) sensing materials employed in electrochemiluminescence; and (IV) photoredox catalysts for organic reactions.

Caption List

Scheme **1**. Synthesis of **4PyCzBP** and **3PyCzBP**. Reagents and conditions: [a] MeCN, 273 to 298 K, 2 h. [b] DMF, KO^{t}Bu (1 equiv.), 150 °C, 19 h. [c] 1,4-dioxane:H_2O (4:1 v/v), Cs_2CO_3 (6 equiv.), $Pd(PPh_3)_4$ (0.1 equiv.), 110 °C, 48 h. All reactions were conducted under an N_2 atmosphere.

Fig. **1** Structure of TADF emitters and corresponding DFT calculated HOMO and LUMO electron density distribution.

Fig. **2** Photophysical properties of a) **3PyCzBP** and b) **4PyCzBP**, normalised UV-Vis spectrum of collected in MeCN at 298 K (blue line) and normalised emission spectra collected in DCM at

298 K (dashed orange line), in MeCN at 298 K (dotted red line) and as spin-coated PMMA-doped films (green) (10 wt%) on quartz substrate.

Fig. **3** Normalised fluorescence and phosphorescence emission spectrum of a) **3PyCzBP** and b) **4PyCzBP** on PMMA-doped film formed (10 wt % of compound) by spin-coating deposition on quartz substrate. Fluorescence and phosphorescence spectra measured at 293 and 77 K, respectively and phosphorescence spectra are measured with a 10 μs delay time.

Fig. **4** a) Emission decay of **3PyCzBP** and **4PyCzBP** collected at 300 K (λ_{exc} = 378 nm) in PMMA-doped thin films (10 wt% of emitter), b) Emission decay of **4PyCzBP** (λ_{exc} = 378 nm) collected as PMMA-doped thin film (10 wt% of emitter) at 77 K (in blue), at 150 K (in yellow), at 200 K (in grey) and at 300 K (in orange). Thin films are formed by spin-coating deposition on quartz substrate.

Fig. **5** Schematic representation of the devices A and B (left) and chemical structures of the materials used in the devices (right).

Fig. **6** Electroluminescent performance of devices A and B: a) EQE vs luminance, b) luminance vs current efficiency and power efficiency.

Fig. **7** Electroluminescence spectra of devices A and B measured at 10 V. The inset shows the photograph of device A.

Fig. **8** Cyclic voltammogram (CV), black, and differential pulse voltammogram (DPV), yellow, of **3PyCzBP** and **4PyCzBP** in MeCN solution, reported versus SCE (Fc/Fc+ = 0.38 V in MeCN).

Fig. **9** Emission decay of **3PyCzBP** (λ_{exc} = 378 nm) collected on PMMA-doped thin film (10 w/w % of compound) formed by spin-coating deposition on quartz substrate at 77 K (in blue), at 150 K (in yellow), at 200 K (in grey) and at 300 K (in orange).

Fig. **10** ^{1}H NMR spectrum of (4-(3,6-dibromo-9H-carbazol-9-yl)phenyl)(phenyl)methanone in $CDCl_3$.

Fig. **11** ^{13}C NMR spectrum of (4-(3,6-dibromo-9*H*-carbazol-9-yl)phenyl)(phenyl)methanone in $CDCl_3$.

812

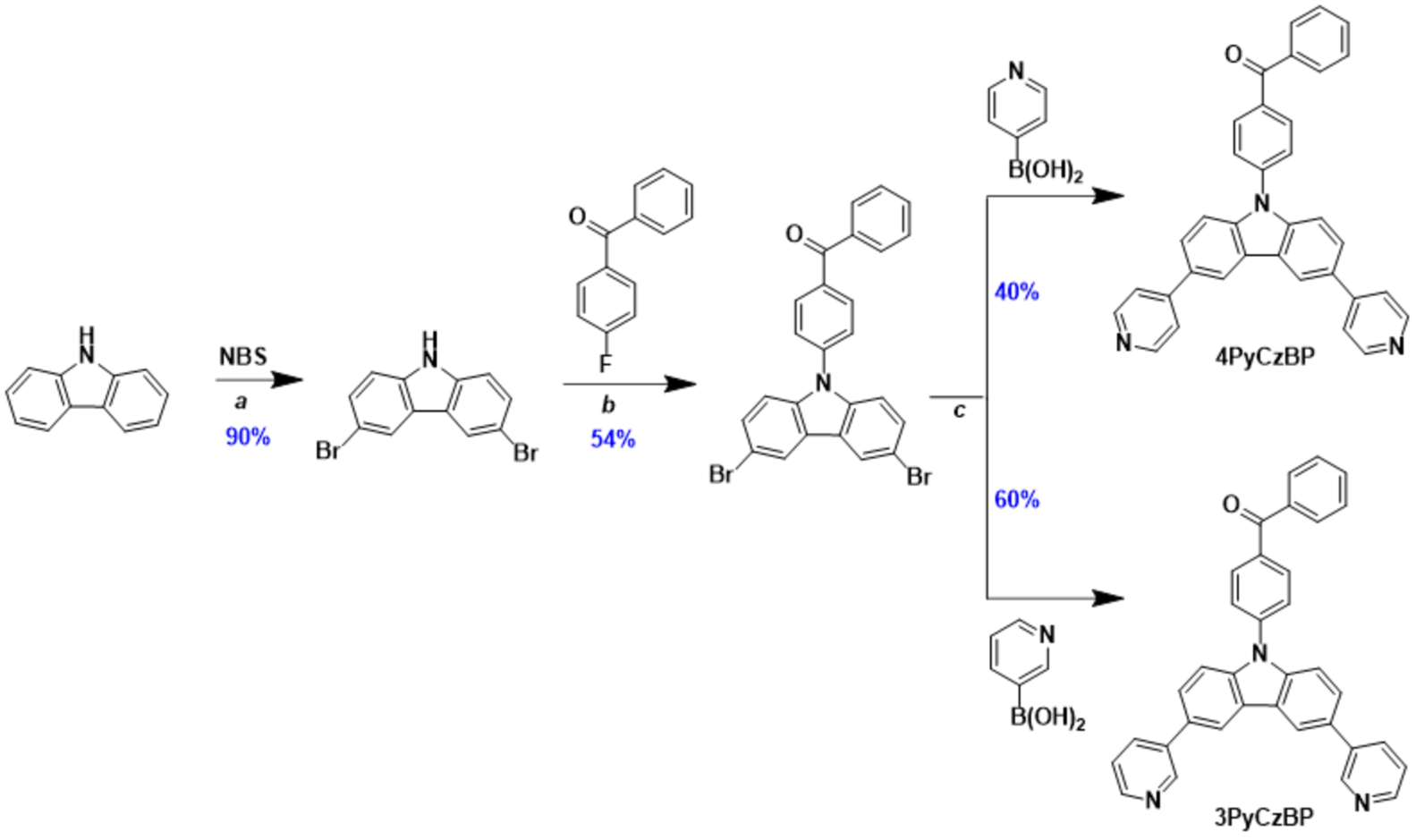
NBS
a
90%
b
54%
c
40%
60%
B(OH)2
B(OH)2
4PyCzBP
3PyCzBP

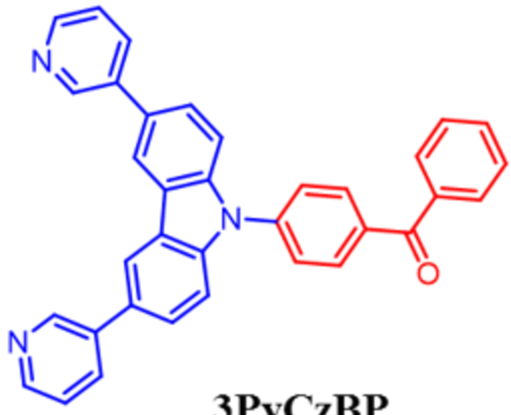

3PyCzBP
ΔE_{ST} = 0.41 eV

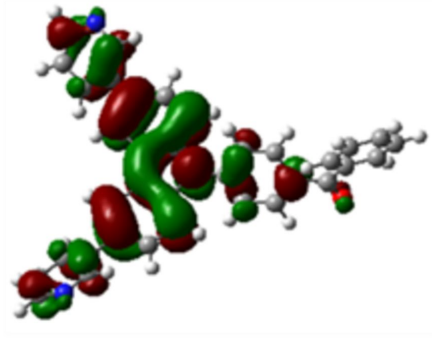

HOMO
5.83 eV

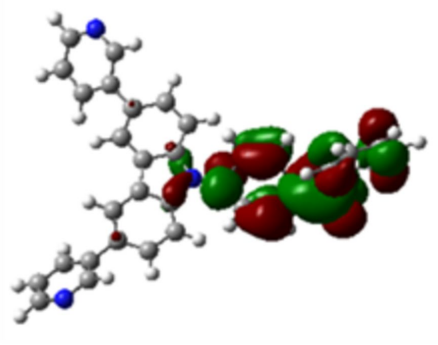

LUMO
1.89 eV

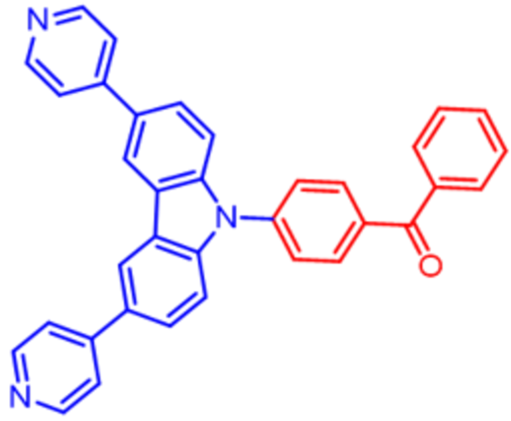

4PyCzBP
ΔE_{ST} = 0.45 eV

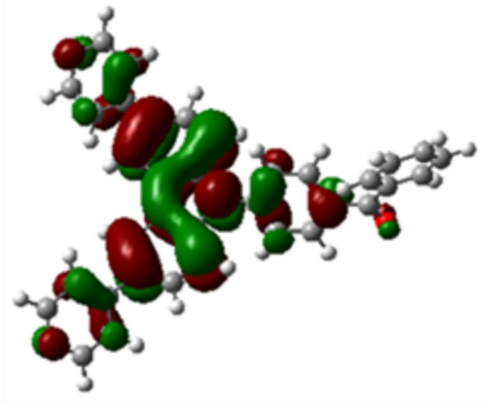

HOMO
5.99 eV

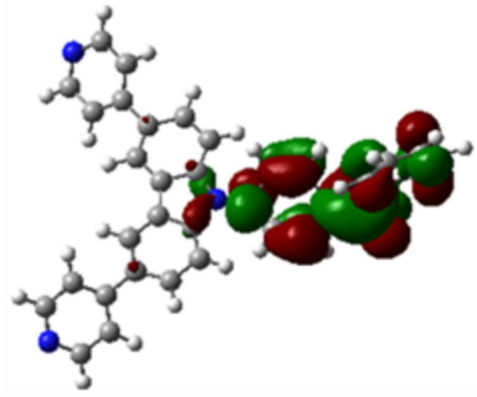

LUMO
1.97 eV

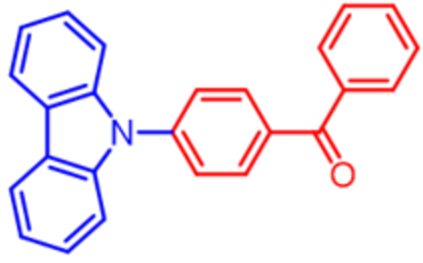

CzBP
ΔE_{ST} = 0.46 eV

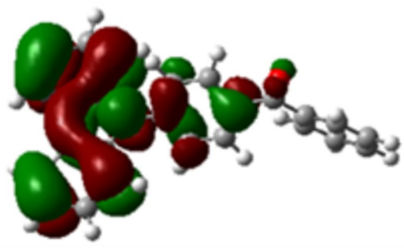

HOMO
5.76 eV

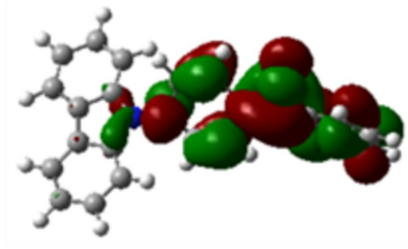

LUMO
1.75 eV

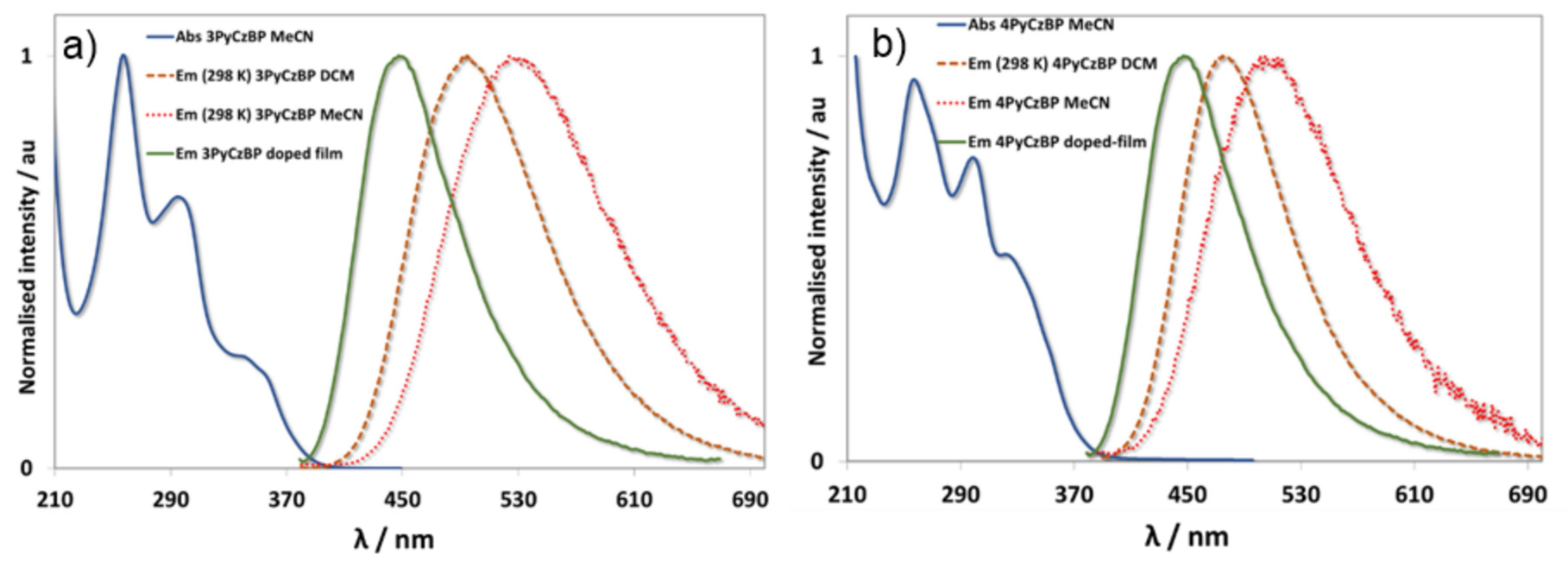
a)
Abs 3PyCzBP MeCN
Em (298 K) 3PyCzBP DCM
Em (298 K) 3PyCzBP MeCN
Em 3PyCzBP doped film
Normalised intensity / au
1
0
210
290
370
450
530
610
690
λ / nm
b)
Abs 4PyCzBP MeCN
Em (298 K) 4PyCzBP DCM
Em 4PyCzBP MeCN
Em 4PyCzBP doped-film
Normalised intensity / au
1
0
210
290
370
450
530
610
690
λ / nm

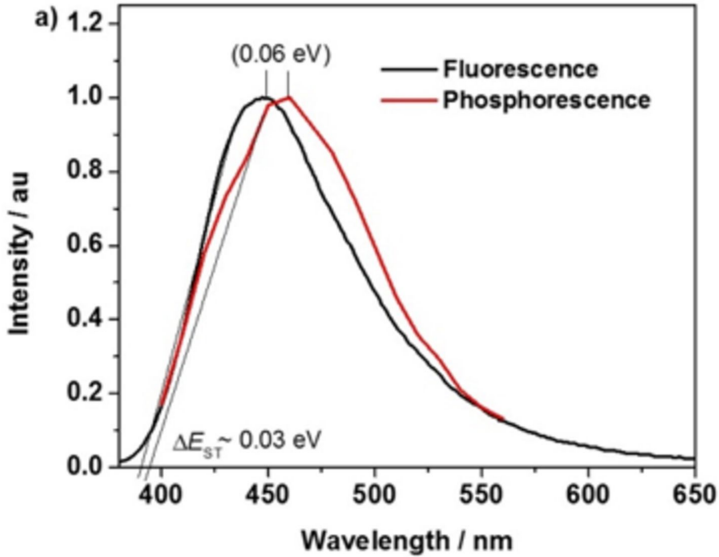
a)
(0.06 eV)
Fluorescence
Phosphorescence
Intensity / au
Wavelength / nm
ΔE_ST ~ 0.03 eV
1.2
1.0
0.8
0.6
0.4
0.2
0.0
400
450
500
550
600
650

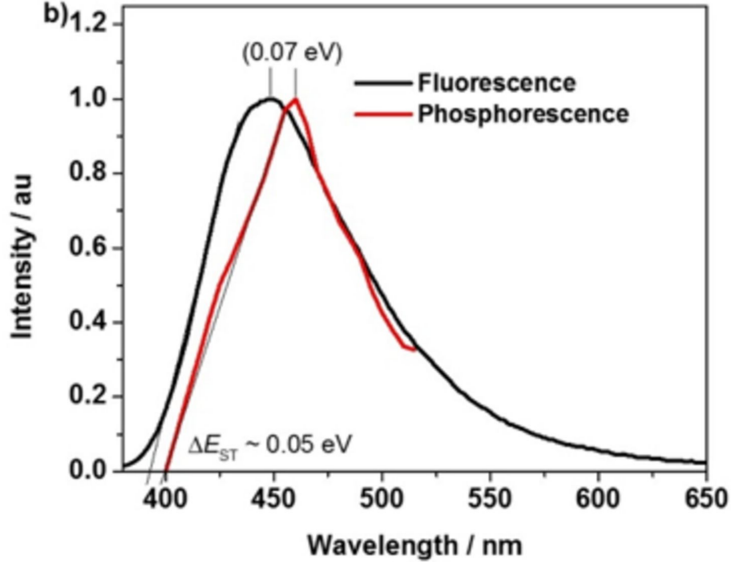
b)
(0.07 eV)
Fluorescence
Phosphorescence
Intensity / au
Wavelength / nm
ΔE_ST ~ 0.05 eV
1.2
1.0
0.8
0.6
0.4
0.2
0.0
400
450
500
550
600
650

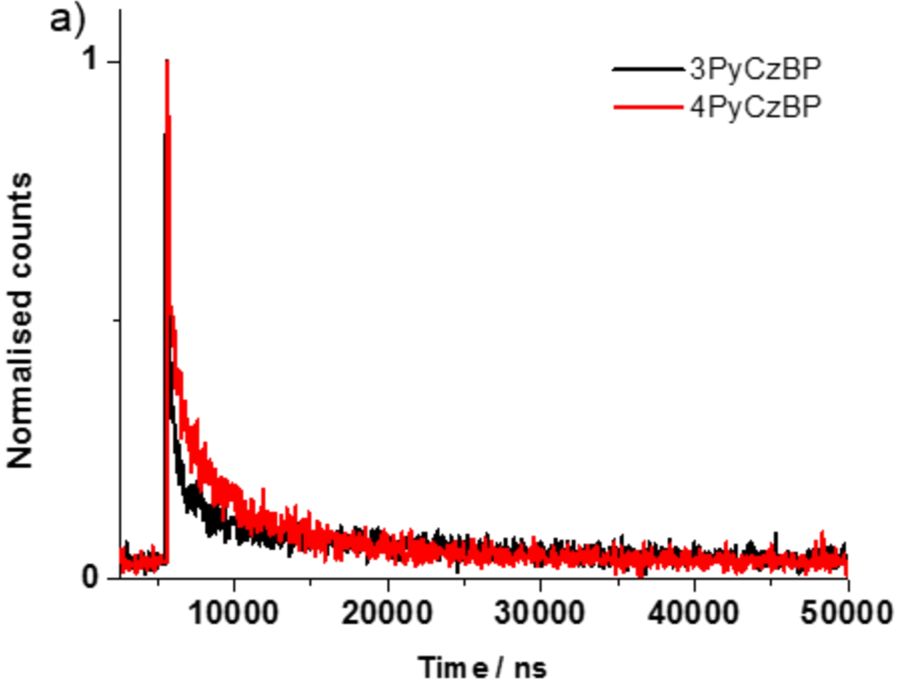
a)
1
0
Normalised counts
3PyCzBP
4PyCzBP
10000
20000
30000
40000
50000
Time / ns

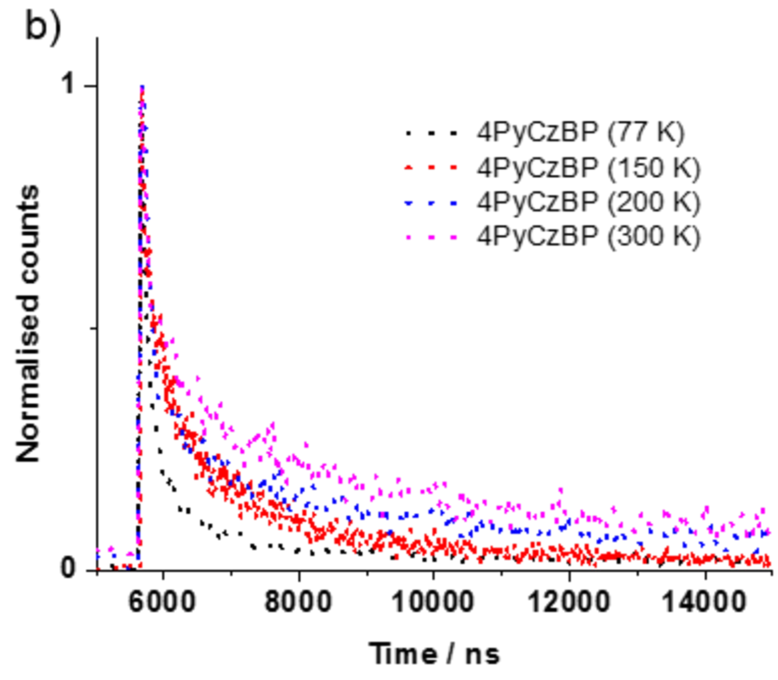
b)
1
0
Normalised counts
4PyCzBP (77 K)
4PyCzBP (150 K)
4PyCzBP (200 K)
4PyCzBP (300 K)
6000
8000
10000
12000
14000
Time / ns

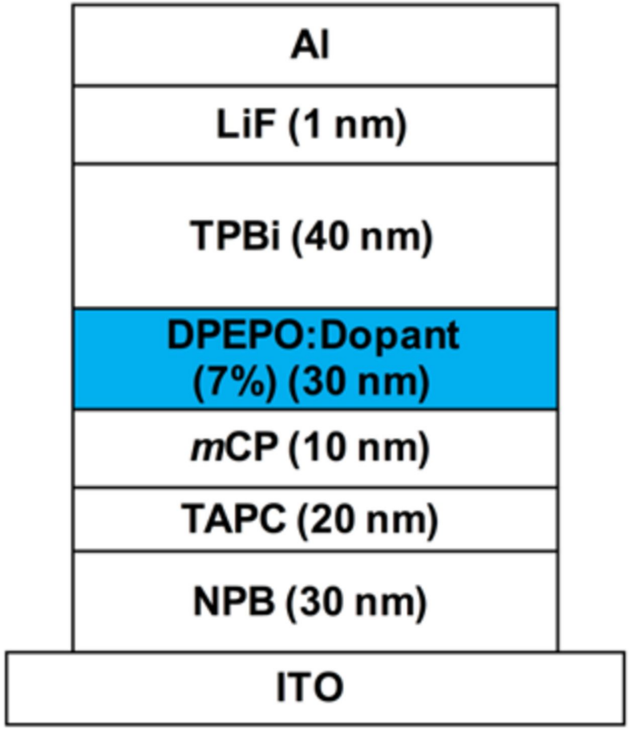

Devices A-B

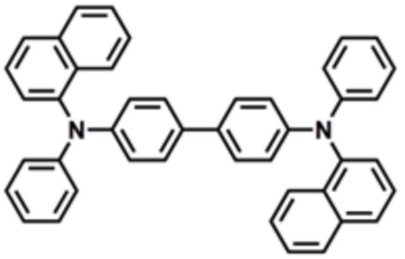

NPB

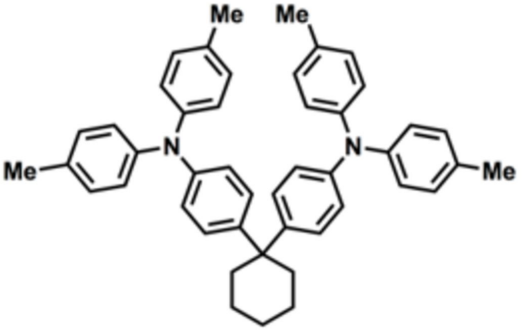

TAPC

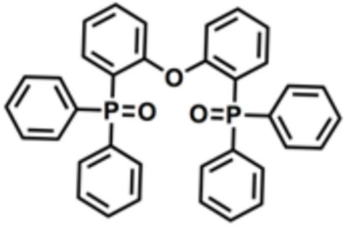

DPEPO

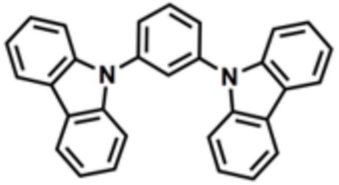

*m*CP

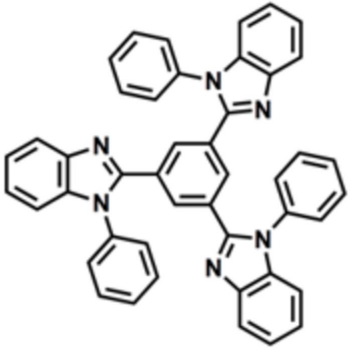

TPBi

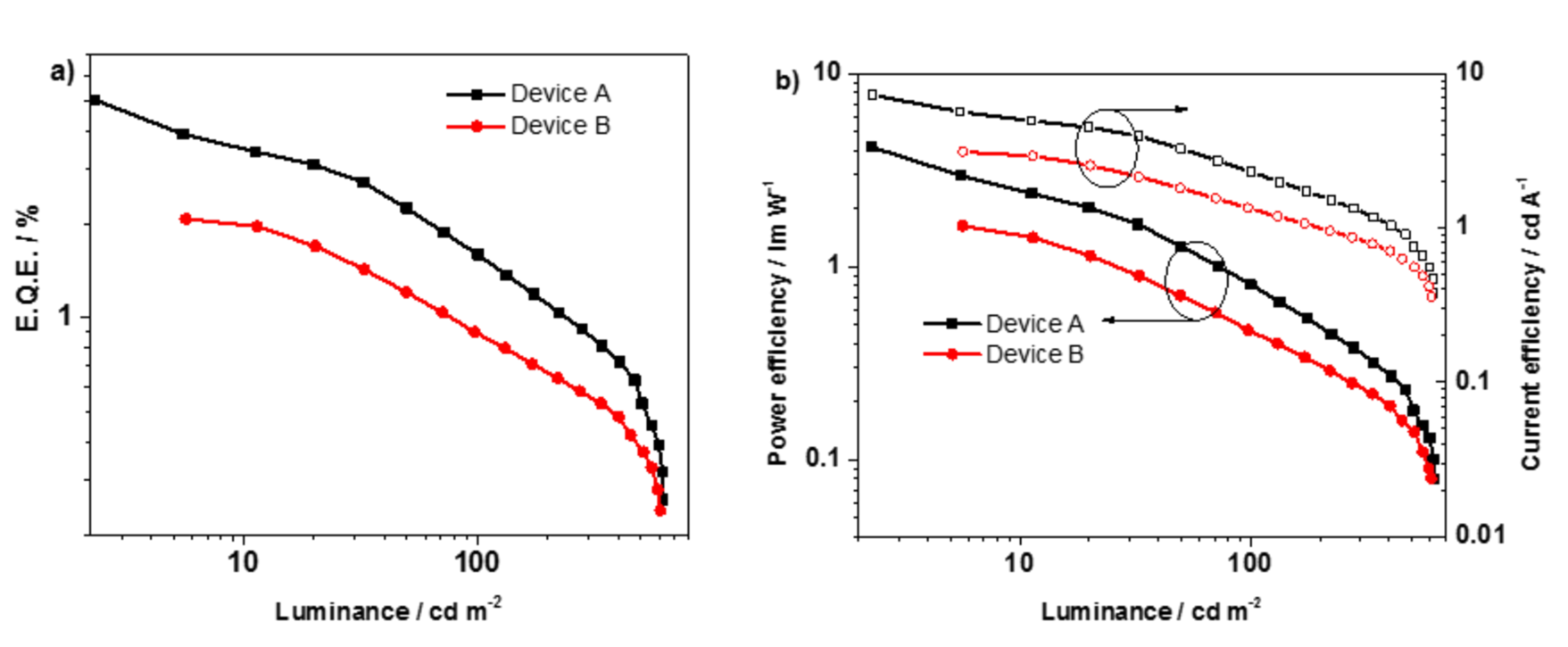
a)
Device A
Device B
E.Q.E. / %
1
10
100
Luminance / cd m-2
b)
10
1
0.1
Power efficiency / lm W-1
Device A
Device B
10
1
0.1
0.01
Current efficiency / cd A-1
10
100
Luminance / cd m-2

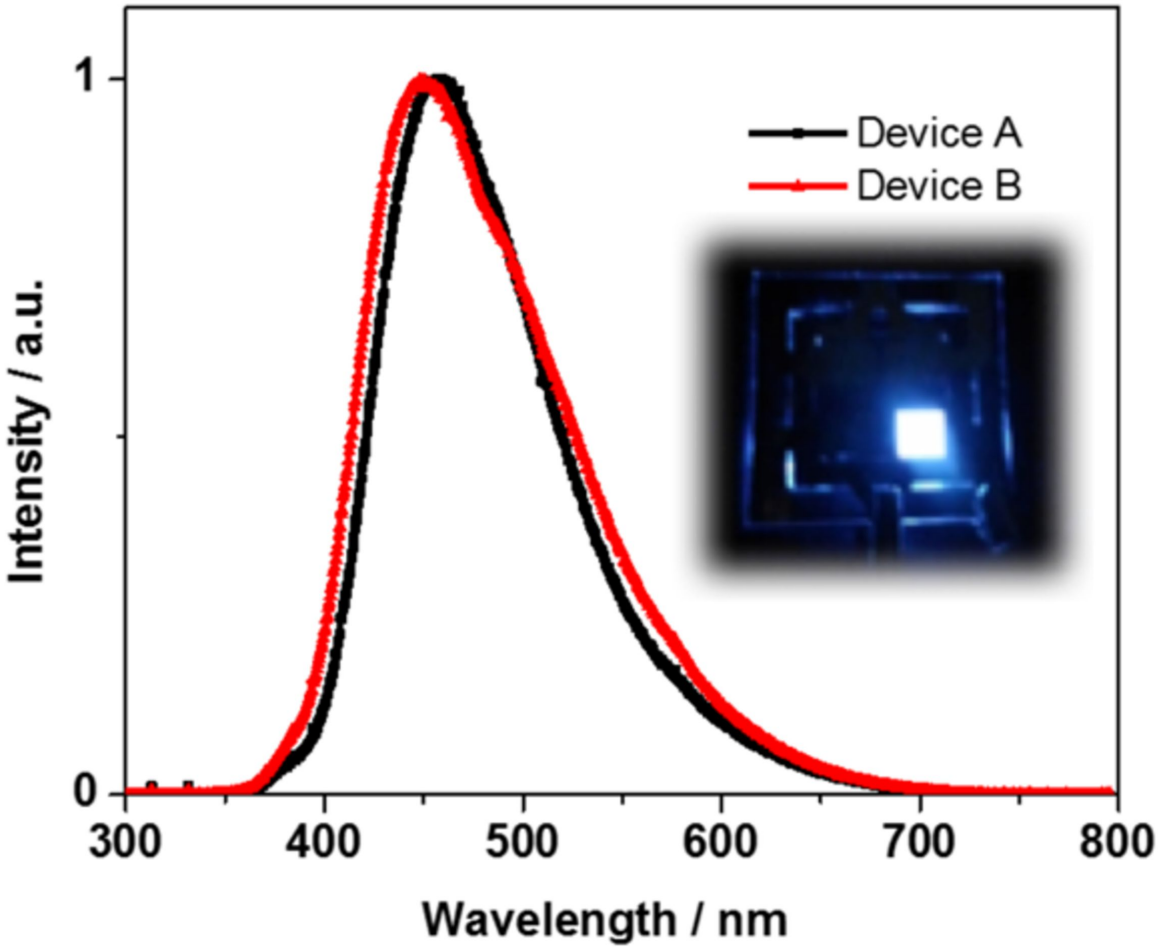
1
0
Intensity / a.u.
300
400
500
600
700
800
Wavelength / nm
Device A
Device B

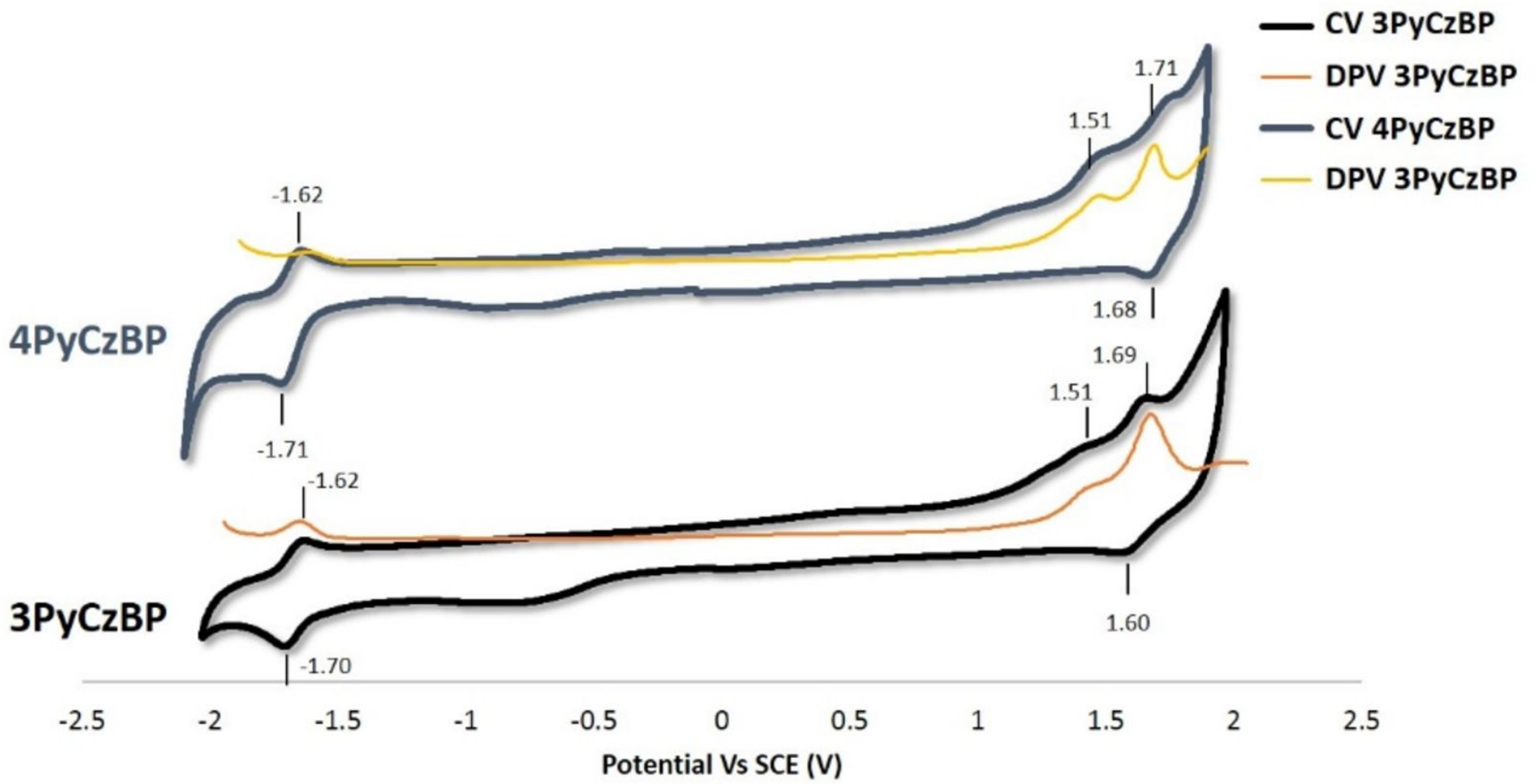
CV 3PyCzBP
DPV 3PyCzBP
CV 4PyCzBP
DPV 3PyCzBP
4PyCzBP
3PyCzBP
1.71
1.51
-1.62
1.68
1.69
1.51
-1.71
-1.62
1.60
-1.70
-2.5
-2
-1.5
-1
-0.5
0
0.5
1
1.5
2
2.5
Potential Vs SCE (V)

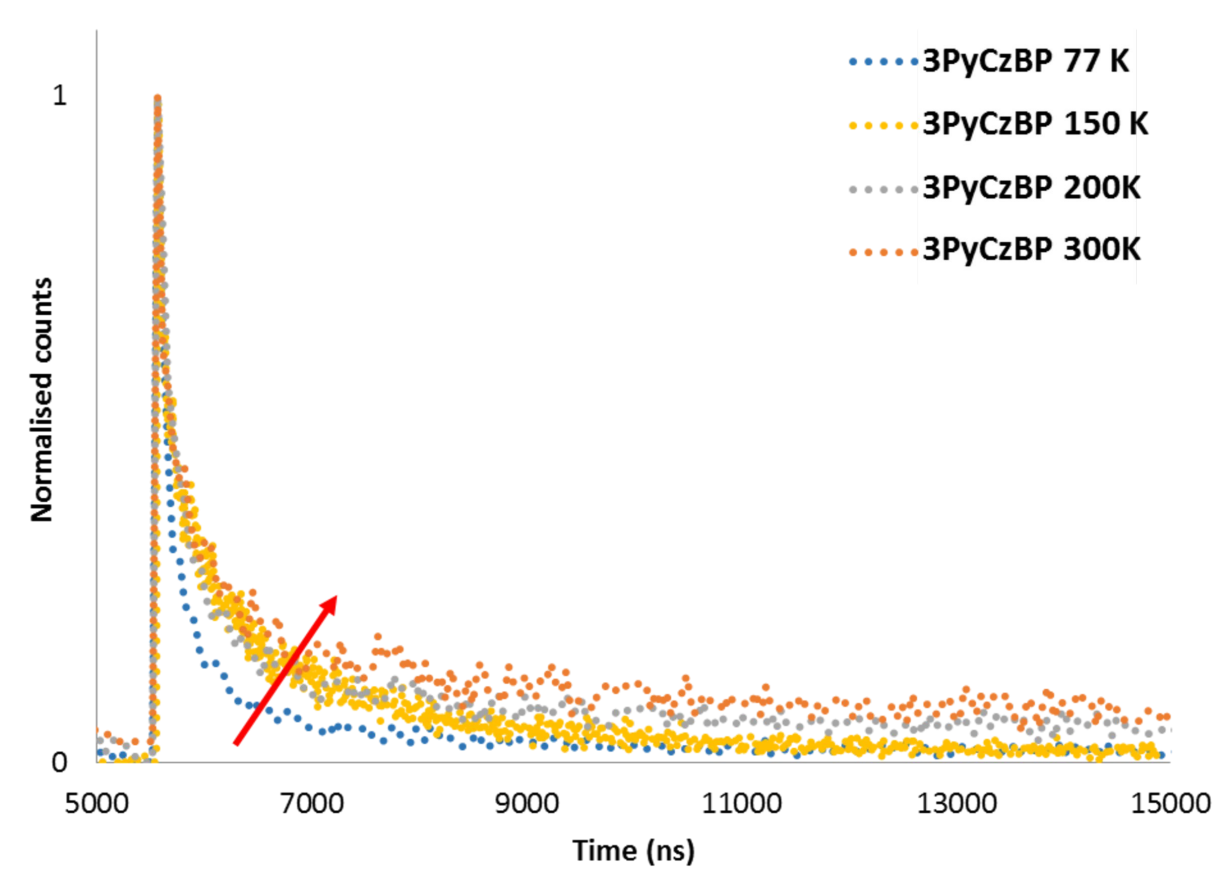
3PyCzBP 77 K
3PyCzBP 150 K
3PyCzBP 200K
3PyCzBP 300K
1
0
Normalised counts
5000
7000
9000
11000
13000
15000
Time (ns)

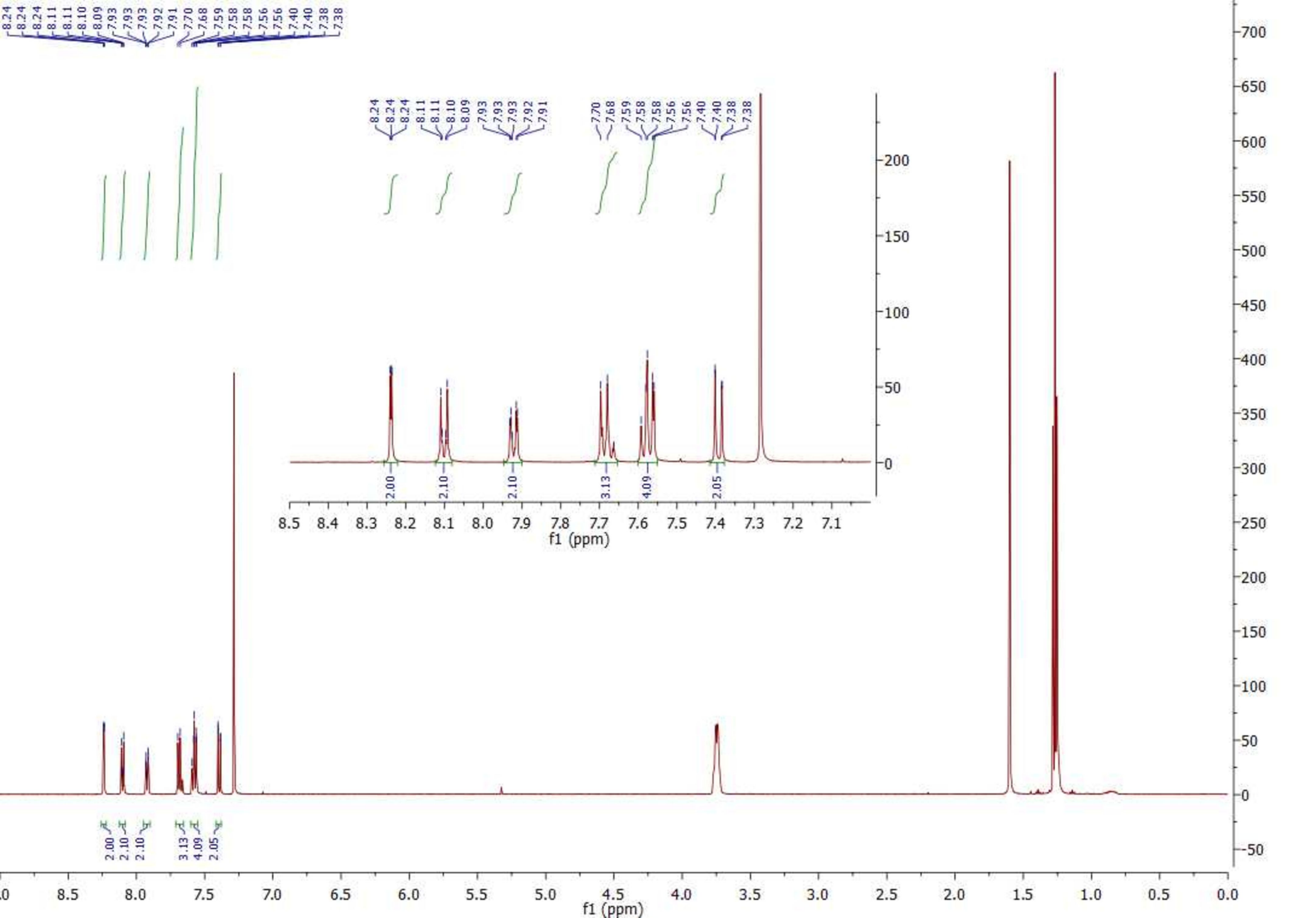
8.24
8.24
8.24
8.11
8.11
8.10
8.09
7.93
7.93
7.93
7.92
7.91
7.70
7.68
7.59
7.58
7.58
7.56
7.56
7.40
7.40
7.38
7.38
2.00
2.10
2.10
3.13
4.09
2.05
f1 (ppm)

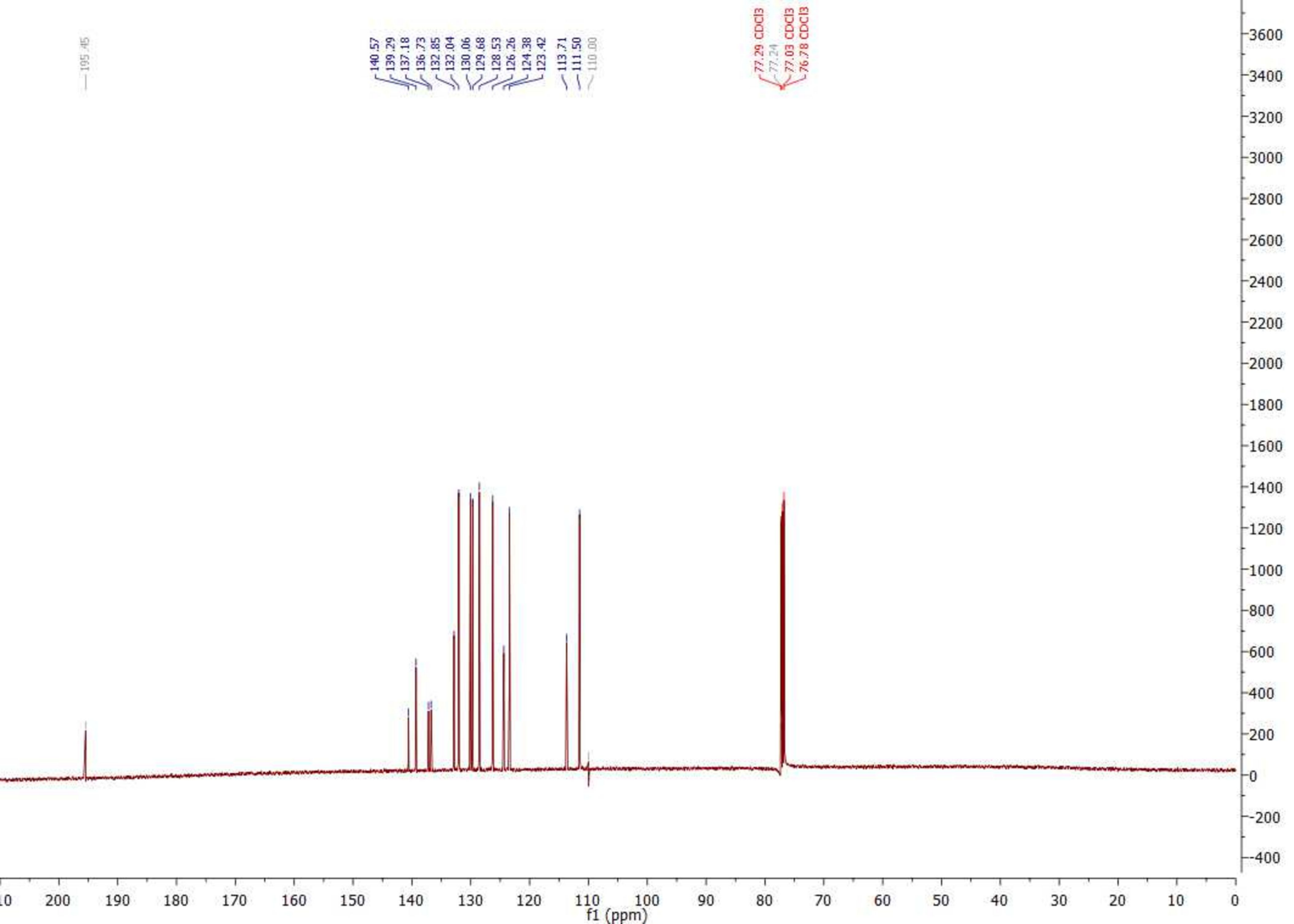
195.45
140.57
139.29
137.18
136.73
132.85
132.04
130.06
129.68
128.53
126.26
124.38
123.42
113.71
111.50
110.00
77.29 CDCl3
77.24
77.03 CDCl3
76.78 CDCl3
f1 (ppm)

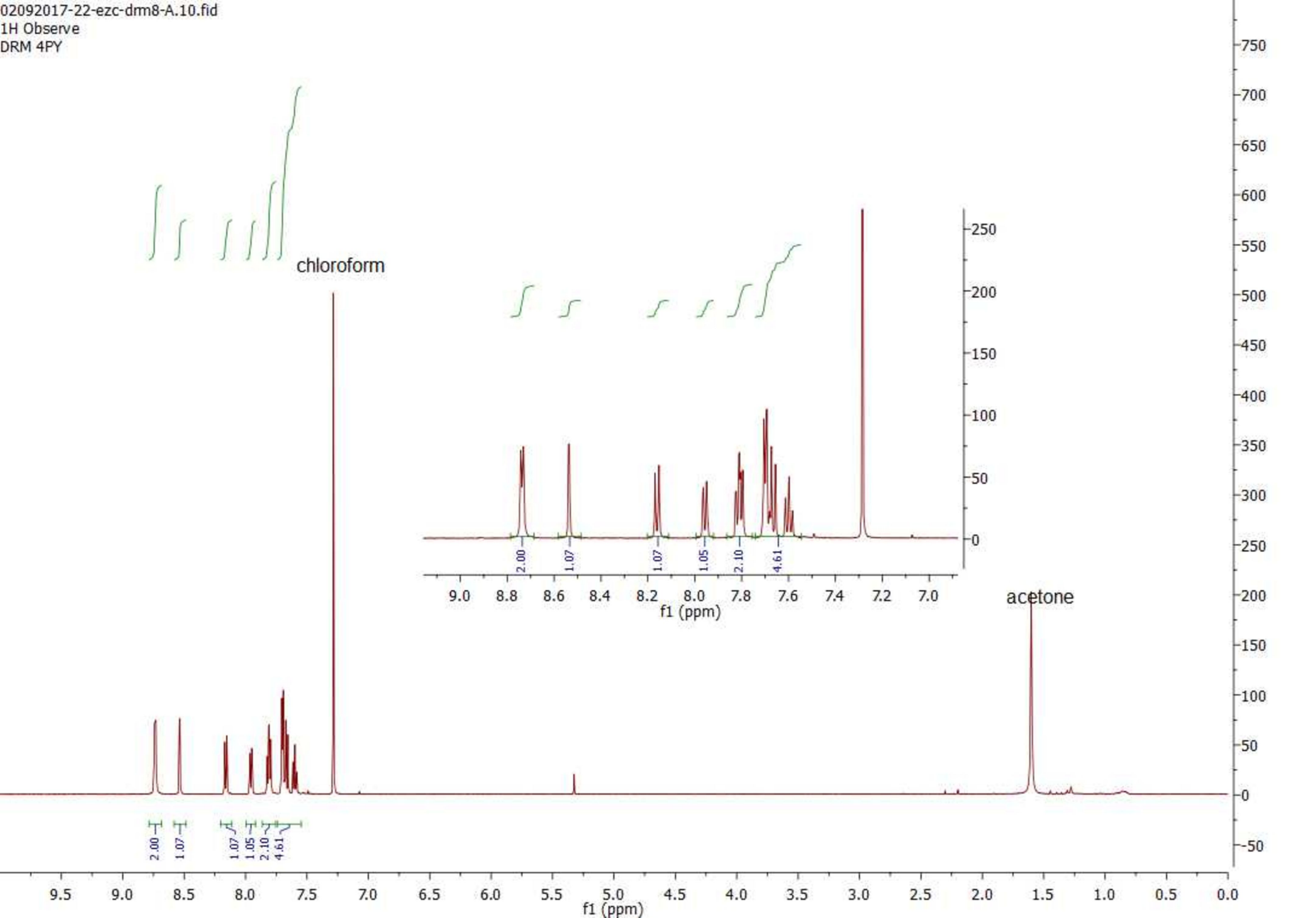
02092017-22-ezc-drm8-A.10.fid
1H Observe
DRM 4PY
chloroform
acetone
2.00
1.07
1.07
1.05
2.10
4.61
f1 (ppm)

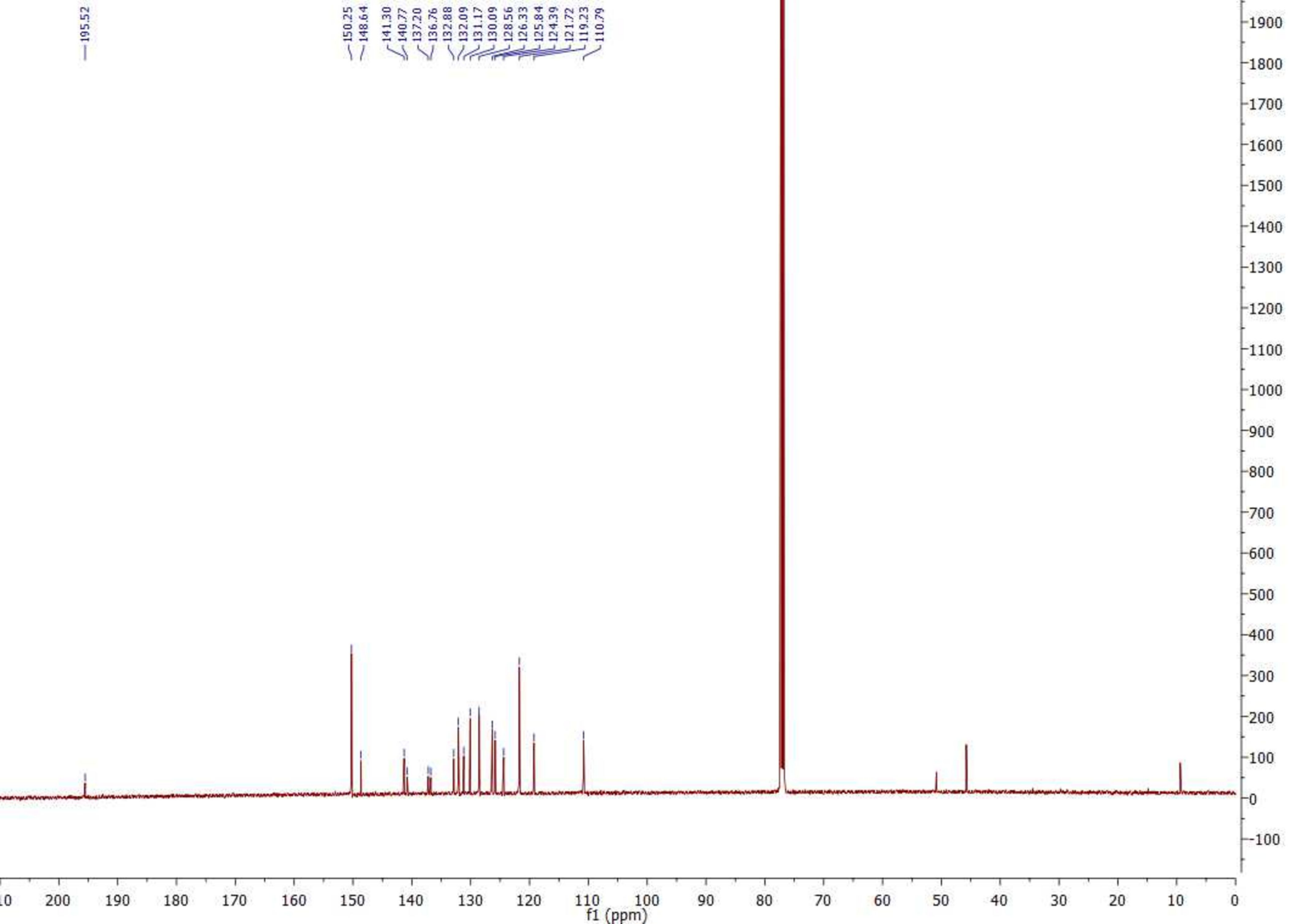
195.52
150.25
148.64
141.30
140.77
137.20
136.76
132.88
132.09
131.17
130.09
128.56
126.33
125.84
124.39
121.72
119.23
110.79
f1 (ppm)

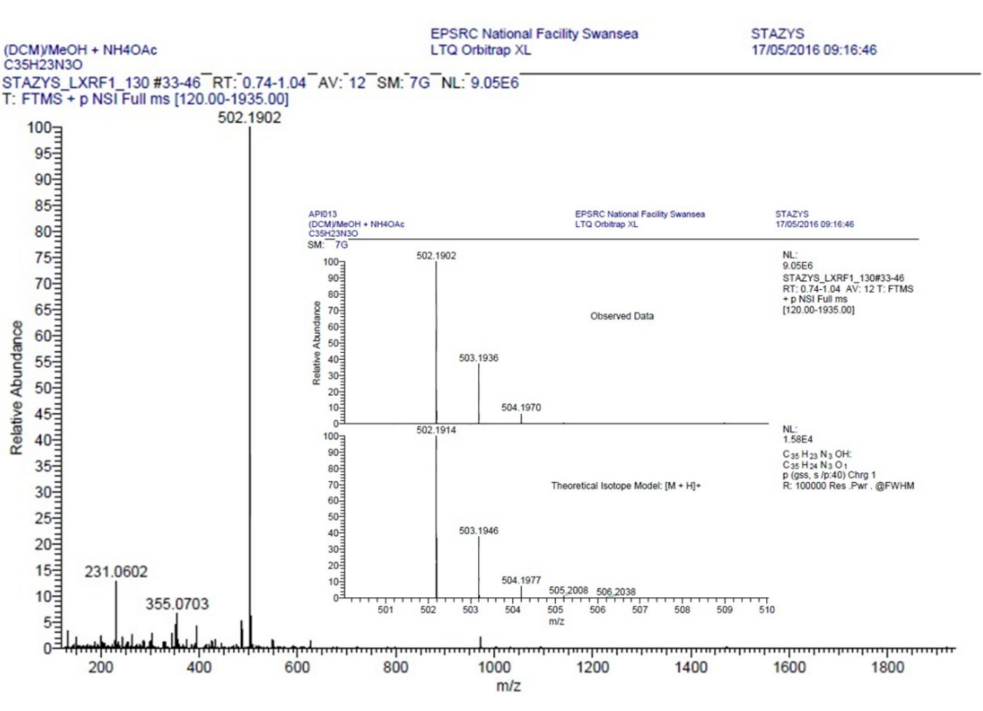
(DCM)/MeOH + NH4OAc
C35H23N3O
EPSRC National Facility Swansea
LTQ Orbitrap XL
STAZYS
17/05/2016 09:16:46
STAZYS_LXRF1_130 #33-46 RT: 0.74-1.04 AV: 12 SM: 7G NL: 9.05E6
T: FTMS + p NSI Full ms [120.00-1935.00]
502.1902
231.0602
355.0703
Relative Abundance
m/z
API013
(DCM)/MeOH + NH4OAc
C35H23N3O
SM: 7G
Observed Data
502.1902
503.1936
504.1970
NL:
9.05E6
STAZYS_LXRF1_130#33-46
RT: 0.74-1.04 AV: 12 T: FTMS
+ p NSI Full ms
[120.00-1935.00]
Theoretical Isotope Model: [M + H]+
502.1914
503.1946
504.1977
505.2008
506.2038
NL:
1.58E4
C35 H23 N3 OH:
C35 H24 N3 O1
p (gss, s /p 40) Chrg 1
R: 100000 Res .Pwr. @FWHM

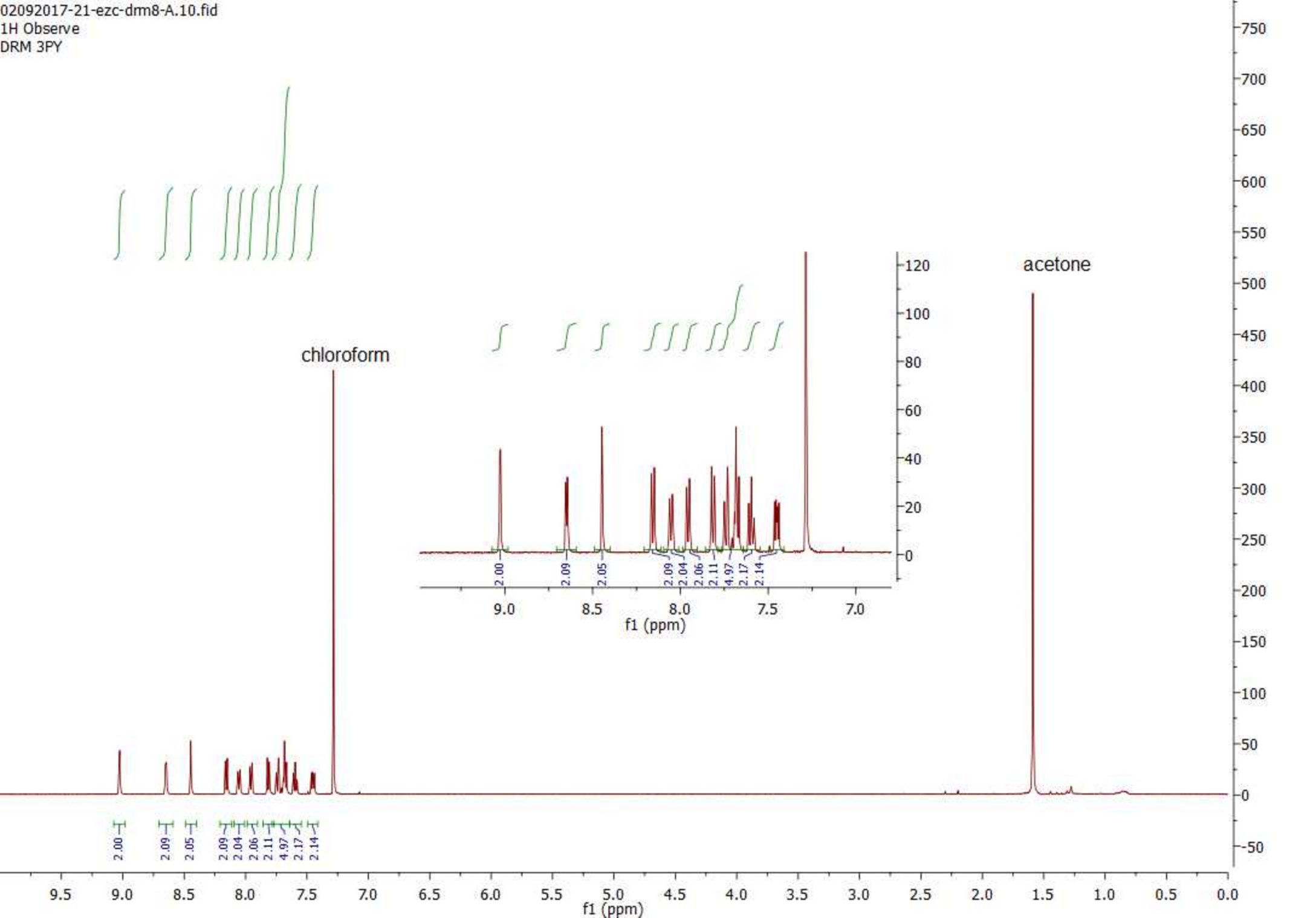
02092017-21-ezc-drm8-A.10.fid
1H Observe
DRM 3PY
chloroform
acetone
2.00
2.09
2.05
2.09
2.04
2.06
2.11
4.97
2.17
2.14
f1 (ppm)

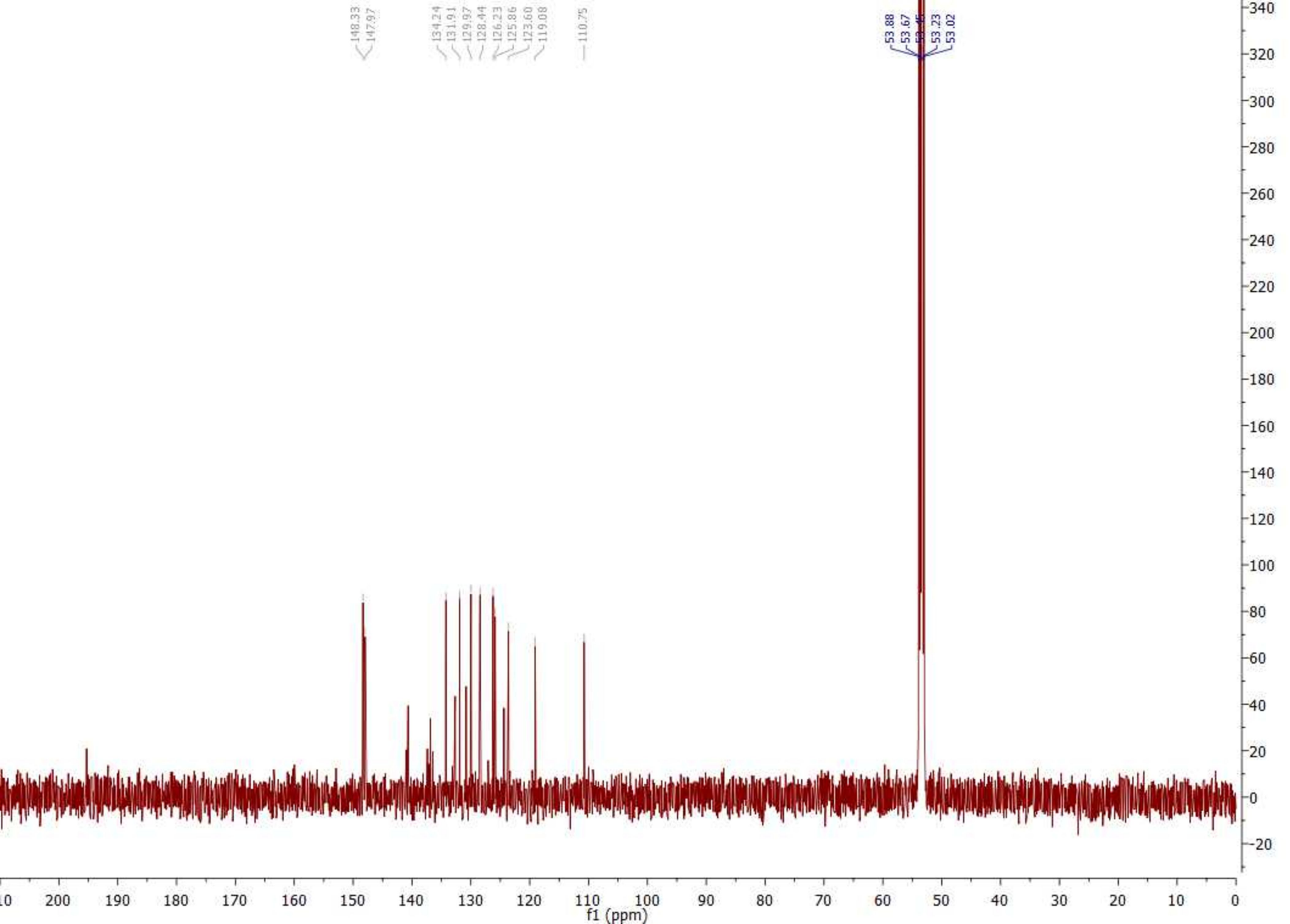
148.33
147.97
134.24
131.91
129.97
128.44
126.23
125.86
123.60
119.08
110.75
53.88
53.67
53.45
53.23
53.02
340
320
300
280
260
240
220
200
180
160
140
120
100
80
60
40
20
0
-20
200
190
180
170
160
150
140
130
120
110
100
90
80
70
60
50
40
30
20
10
0
f1 (ppm)

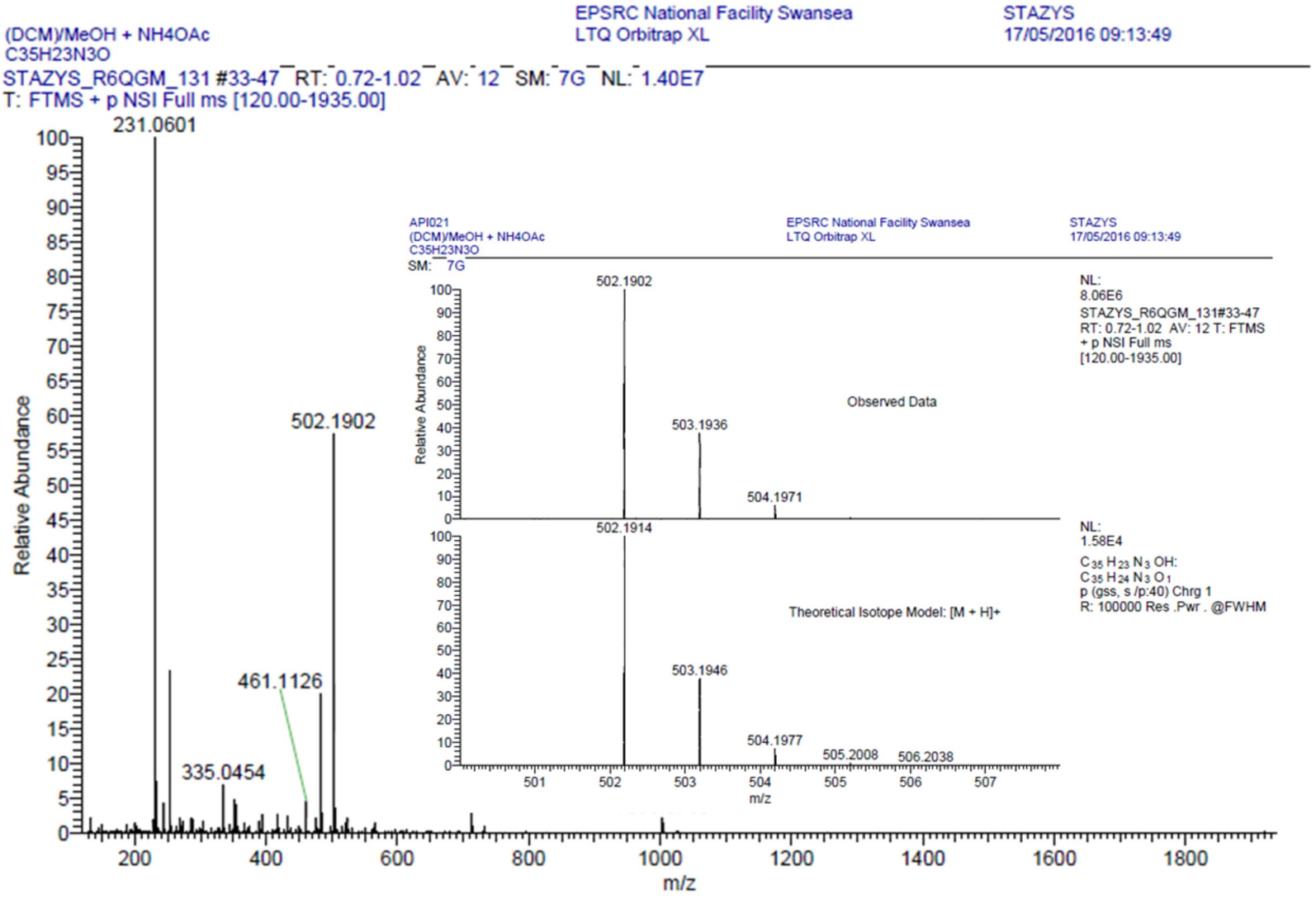
(DCM)/MeOH + NH4OAc
C35H23N3O
EPSRC National Facility Swansea
LTQ Orbitrap XL
STAZYS
17/05/2016 09:13:49
STAZYS_R6QGM_131 #33-47 RT: 0.72-1.02 AV: 12 SM: 7G NL: 1.40E7
T: FTMS + p NSI Full ms [120.00-1935.00]
231.0601
502.1902
461.1126
335.0454
Relative Abundance
m/z
API021
(DCM)/MeOH + NH4OAc
C35H23N3O
SM: 7G
Observed Data
502.1902
503.1936
504.1971
NL:
8.06E6
STAZYS_R6QGM_131#33-47
RT: 0.72-1.02 AV: 12 T: FTMS
+ p NSI Full ms
[120.00-1935.00]
Theoretical Isotope Model: [M + H]+
502.1914
503.1946
504.1977
505.2008
506.2038
NL:
1.58E4
C35 H23 N3 OH:
C35 H24 N3 O1
p (gss, s /p:40) Chrg 1
R: 100000 Res .Pwr . @FWHM